Fall 2008

Synthesis of iron oxide nanoparticles in a counterflow diffusion flame reactor

Hector Enrique Ruiz

Department:

SYNTHESIS OF IRON OXIDE NANOPARTICLES IN A COUNTERFLOW DIFFUSION FLAME REACTOR

by

HECTOR ENRIQUE RUIZ

A THESIS

Presented to the Faculty of the Graduate School of the

MISSOURI UNIVERSITY OF SCIENCE And TECHNOLOGY

In Partial Fulfillment of the Requirements for the Degree

MASTER OF SCIENCE IN CHEMICAL ENGINEERING

2008

Approved by

Dr. Yangchuan Xing, Advisor

Dr. Douglas K. Ludlow

Dr. F. Scott Miller

ABSTRACT

A Counterflow Diffusion Flame (CDF) reactor was used to produce iron oxide nanoparticles. The experimental work was performed to study synthesis conditions and characterize the iron oxide nanoparticles. The parameters studied are those that control the flame structure, namely, gas flow rates and vacuum; other parameters include the precursor volume flow rate, and the relative location and temperature of the collecting probe inside the flame.

Hexagonal nanoparticles were the most commonly observed shape. Hexagonal-shaped nanoparticles are mainly formed under stoichiometric conditions and with a high temperature profile in the flame. Cubic nanoparticles were also observed. The main parameter for the formation of cubic-shaped nanoparticles was found to be the equivalence ratio. A minimum value of less than one percentage of cubic nanoparticles was observed at equivalence ratios ranging between 0.7488 and 0.9283.

The main effect on particle size was observed to be from the hydrogen flow rate, which was found that the higher the hydrogen flow rate is, the smaller the average nanoparticle size. A secondary minor effect was observed from variations of vacuum flow rate. This effect could be associated with changes in the total mass or volumetric flow rate balance. Adjusting N_2 in H_2 stream allowed the synthesis of samples with approximately 95% hexagonal nanoparticles without agglomerates.

ACKNOWLEDGMENTS

Thanks to Dr. Yangchuan Xing for his support and guidance. Further, I also want to acknowledge the National Science Foundation for partially funding this research.

Thanks to Dr. Douglas K. Ludlow and Dr. F. Scott Miller for serving on my graduate committee and their guidance and understanding.

Finally, thanks to my friends and family for their understanding and encouragement during this study.

TABLE OF CONTENTS

LIST OF ILLUSTRATIONS

LIST OF TABLES

1. INTRODUCTION

Nanotechnology is the creation and utilization of materials, devices, and systems through the control of matter on the nanometer-length scale that is at the level of atoms, molecules and supramolecular structures [1]. In recent years nanotechnology has seen an exponential growth in both applications and research for new nanomaterials. Nanotechnology is called the technology of the 21st century [2].

The goal of the present study is to evaluate the synthesis conditions and characterize the iron oxide nanoparticles produced in a CDF reactor according to variations of the parameters that control the flame structure.

Iron oxide nanoparticles have been used in biomedical imaging applications. Superparamagnetic iron oxide nanoparticles (SPIONs) have been used for many years, for example, nonviral gene delivery, MRI contrast agents, and separation applications [2]. Also iron oxide nanoparticles have been used in applications for optical-magnetic recording [3].

Several methods for production of iron oxide nanoparticles are reported in the literature [4-9]. According to the nature of the synthesis methods, the current literature can be divided into liquid phase synthesis methods, and gas phase and aerosol synthesis methods. Most of the reported methods of iron nanoparticle synthesis are based on aqueous or liquid synthesis, and few methods reported are based on gas or aerosol synthesis at relative high temperatures. The main disadvantage of liquid synthesis methods is the complex chemistry that often should be used eventually limits scalability of the production process. On the other hand, gas phase and aerosol synthesis methods do not need elaborated chemistry procedures and are easier to adapt for continuous production. The present study will focus on the synthesis and characterization of iron oxide nanoparticles in gas or aerosol phase.

1.1. METHODS FOR IRON OXIDE NANOPARTICLES SYNTHESIS

1.1.1. Spray and Laser Pyrolysis Methods. In the spray pyrolysis method, the nanoparticles are formed by decomposition of an aerosol flowing through a hot zone, where aerosol constituents react to form a compound. Homogeneous reaction conditions should prevail in order to obtain nanoparticles. Spray pyrolysis methods have been used to prepare gamma-Fe_2O_3 nanoparticles [4,5]. Gonzalez-Carreno [4] reported obtaining particles with sizes ranging from 5 to 60 nm, the smallest sizes obtained from acetylacetonate solutions and nitrate solutions. The morphology also varied accordingly to the precursor used, namely: hollow spheres of 170 nm using Fe (II) ammonium citrate solutions and high crystalline particles using Fe (III) chloride solutions. In all cases the formation of gamma- Fe_2O_3 phase was observed under the conditions studied. Fairly larger particles (200-500 nm) were prepared by Martinez [5] using spray pyrolysis of Fe (III) and Fe (II) salts, all of which with spherical morphology. They correlated the increase in particle size to the increase of furnace temperature and the decrease of carrier gas flow.

An alternative to the spray pyrolysis method is laser pyrolysis. In this case the laser energy induces the decomposition of the aerosol. Veintemillas [6] reported preparation of pure gamma- Fe_2O_3 nanoparticles by using laser pyrolysis. A continuous process was developed from CO_2 laser induced pyrolysis of solutions of iron pentacarbonyl in isopropanol. Average production rate of 0.05 g/h was obtained, with particle size of 5 ± 2nm, with a low degree of agglomeration and mainly crystallized nanoparticles.

1.1.2. Flame Synthesis Methods. In this method a combustion flame is used as a source of energy to decompose an aerosol flowing trough the flame. The final particle characteristics are determined by fluid mechanism and particle dynamics within a short period of time at the early stages in the synthesis process. During this short timeframe, three major formation mechanisms dominate the particle formation after the initial chemical reaction of the precursor to form monomers (clusters) by homogeneous (gas phase) nucleation [7]

- Growth of particles by reaction of the precursor on the newly formed particles (surface growth)

- Coagulation if high particle concentrations are present due to the Brownian motion, particles collide and if adhesive forces are strong, these collision results in coagulation.
- Finally, coalescence and fusion can play an important role in high temperature zones due to sintering process

Zachariah et al. [8] reported the conditions for fabrication of iron oxide-silica nanoparticles up to 10 nm in size with superparamagnetic properties using a flame methane-oxygen flame reactor. The particle size was control by variations of the precursor rate. Basically spherical particles were formed under high temperature (>2000 K) at rates of up to 2g/h.

Xing, et al. [9] reported the synthesis of shape-controlled nanoparticles by using a CDF reactor. Xing et al tested flames composed of hydrogen-argon and oxygen-argon opposite flow streams. The relative concentration of Ar was used to adjust the mass flow rate. The equivalent ratio (defined as the ratio of actual molar ratio of hydrogen to oxygen to the stoichiometric molar ratio for complete combustion) was constant. Two momentum ratios (defined as the ratio of momentum between hydrogen/oxygen streams) were used, setting the gas stagnation plane as close to the flame as possible. They analyzed the particles by the Transmission Electron Microscopy (TEM) and the results clearly show an evolution of nanoparticles formed in the flame. Initially, aggregates with undefined shapes are formed, as they flow toward the flame they collapse and restructure into single nanoparticles. Experimental results show a variety of crystallographic shape nanoparticles. When chemical precursor was fed at the hydrogen stream, mainly hexagonal shapes were observed. When the precursor was fed to the oxygen stream, cubic nanoparticles were formed. Similar nanoparticle shape evolution has been observed previously for aluminum [10] but without formation of different crystallographic shapes.

Xing et al. [9] describe the chemical environment in the CDF as follows (see Figure 1.1):

- On the hydrogen side, hydrogen concentration is maximum at the entrance of the bottom channel and approaches zero at the flame.

- H_2O generates at the flame therefore its concentration is max at this zone, decreasing its concentration toward each channel entrance.

- In the hydrogen side, major radicals of OH and H are produced close to the flame. They do not survive low temperature regions. Only H_2O vapor is available to react with precursor at the channel entrance.

- In the oxygen side, O_2, H_2O, OH and H_2O are present to react with the precursor at the channel entrance.

They reported that the difference in chemical environment is the main cause of difference in shape of iron oxide nanoparticles.

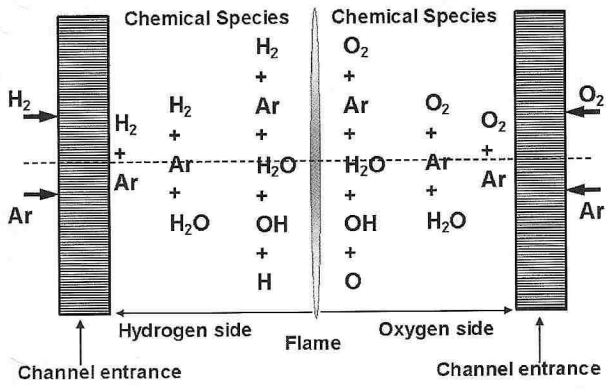

Figure 1.1. Cross-section view of major chemical species in the CDF reactor [9].

Rumminger and Linteris [11] reported that thermophoresis affects the iron oxide nanoparticle distribution in the counterflow diffusion flames, in some cases causing particles to cross the stagnation plane. The scattering magnitude of the particles in the counterflow diffusion flames appears to be strongly dependent on the residence time, and rather independent of the peak flame temperature.

Guo and Kennedy [12] reported the synthesis of iron oxide nanoparticles in a H_2/air diffusion flame. They used H_2 flow rate of 0.2 l/min and a $Fe(CO)_5$ vapor concentration of about 500 ppm, collecting on a filter typically 5 mg of sample per hour. That particular synthesis condition produced a particle size distribution obtained that contained two size modes, namely, 45 and 3-8 nm. Smaller sizes appeared forming agglomerates. The median particle size for the large size mode increased with higher

$Fe(CO)_5$ concentration but the primary diameter for the smaller mode did not change significantly. Particles in the large size mode were fully crystallized while those in the smaller size mode were amorphous. They proposed a formation mechanism for both size modes that describe the pyrolysis of $Fe(CO)_5$ in the reducing atmosphere of the fuel side. As the iron moves along the flame axis, the oxygen concentration increases as well as the temperature. Iron is then oxidized into FeO. Next, at the maximum temperature region liquid FeO converts to vapor-phase FeO. After passing the hot flame gases temperature decreases and the FeO and Fe vapors nucleate to form small particles and convert into Fe_2O_3 due to super-stoichiometric oxygen concentration. The remaining liquid FeO convert to Fe_2O_3 because of increased oxygen partial pressure and form larger particles.

1.1.3. Flame's temperature profile measurements. The temperature measurements of the hot gases in the CDF reactor are important to explain the nanoparticle formation mechanism. Temperature-distance data can provide the key characteristic profile of a flame because most of the parameters of nanoparticle formation in the flame are temperature dependent. Among the methods for flame temperature measurements, they fall in two categories namely [13]:

-Optical methods, in which the effect of parts of the flame on radiation passing through them is measured.

- Probe thermometry, in which probes in the form of thermocouples or gas sampling probes are introduced into the flame.

The optical methods have the advantage that the flame remains undisturbed during measuring, but the measures are integrated over the whole path length of the flame. Thus departures from ideal flatness of the flame may cause difficulty in interpretation [13].

The Probe Thermometry method mainly consists of thermocouple measurements and resistance thermometry. This is the most direct method to measure flame temperatures. The main disadvantages of the method are that it causes aerodynamic disturbances to the flame and needs corrections due to radiation. On the other hand, a detailed point-wise temperature profile can be obtained independently of the flame type [13].

The thermocouple measurement uses the thermoelectrical properties of metals. Source of errors in measuring the true gas temperatures can be mainly due to the effect of the probe itself in the flame. The probe can disturb the aerodynamic, thermal or chemical profile of the flame. These errors can be reduced if the size of the thermocouple is decreased (up to the limit where the thermocouple wire diameter is comparable with the mean free path). Also errors can be reduced when the gas density and velocity is increased (up to the limit where the difference between static and stagnation temperature becomes important). In addition, conduction losses can be reduced in flat flames if supporting wires are aligned with plane of constant temperatures [13]

The radiation correction remains one of the most serious sources of error for the probe thermometry method. The thermocouple could be at lower or higher temperature than the gas. Temperature radiation from the surroundings could yield higher temperatures up to several orders of magnitude. One method to correct this is by electrical heating the thermocouple. The problem with the electrical correction is that the voltage range needed for heating can be large compared to the voltage produced by the thermojunction causing loss of accuracy. Another way to account for radiation is by using a suction pyrometer [14]. Suction pyrometers (see Figure 1.2) do not measure gas temperature directly. Two temperatures are measured and the gas temperature is calculated from them. First, the temperature is measured when non-gas flow trough the pyrometer; known as the non-suction temperature (Θ_{ns}). A second temperature is measured under a predetermined gas flow; known as the suction temperature (Θ_s). The suction pyrometer allows obtaining the relation between these two temperatures and the true gas temperature (Θ_g) can be obtained using the following equation:

$$\Theta_g = \Theta_{ns} + (\Theta_s - \Theta_{ns})/e \qquad (1)$$

Where "e" is known as the efficiency of the pyrometer. The efficiency e can be calculated from the dynamic response of the pyrometer to sudden changes in gas flow.

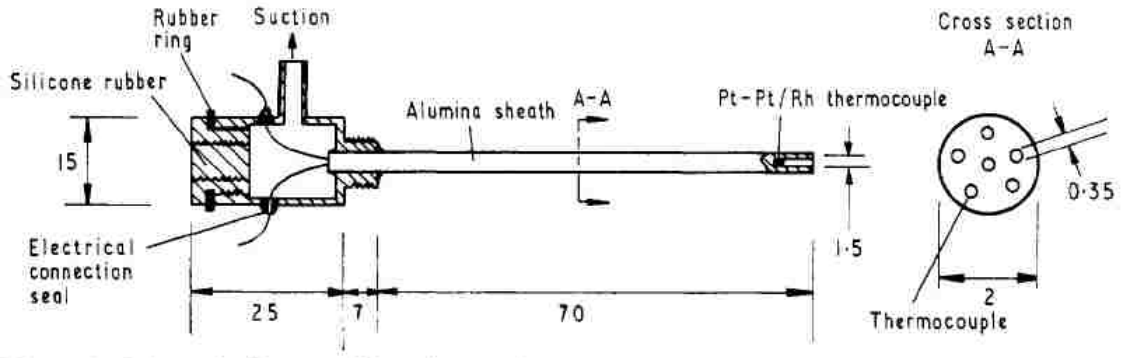

Figure 1.2. Schematic diagram of the microsuction pyrometer (all dimension in mm) [12].

The true temperature of the gas can also be estimated by using a series of thermocouples with different bead diameters. The following equation relates the balance between the heat convected to the bead and the heat radiated from it [14]:

$$\Theta_b = \Theta_g + (d_s/(2+f(Re))\beta \qquad (2)$$

Where θ_b is the temperature at the bead, θg is the gas temperature, d_b is the diameter of the bead, β is constant and f(Re) is the so call view factor dependent on the Reynolds number Re. At the limit when $d_b \Rightarrow 0$, $\theta_b = \theta_g$. Figure 1.3 shows the extrapolated value of true gas temperature from reference [14].

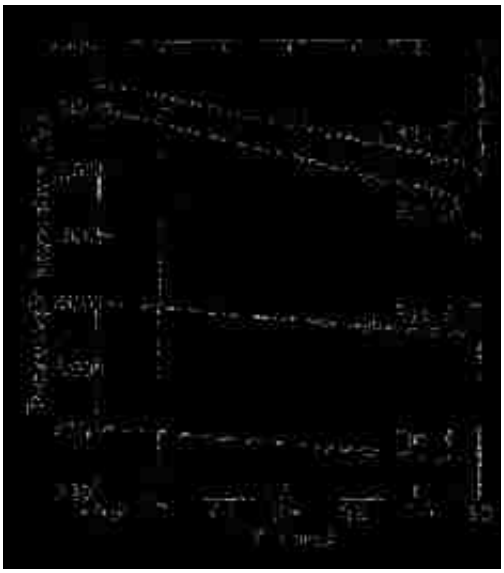

Figure 1.3. Variation of the thermocouple temperatures with the bead diameter: crosses, measured gas temperature; circles, extrapolated value of true gas temperature [12].

2. EXPERIMENTAL SETUP

2.1. THE COUNTERFLOW DIFFUSION FLAME REACTOR (CDF)

A CDF reactor was used to produce and study the iron oxide nanoparticles. Figure 2.1 shows a schematic drawing of the CDF reactor and Figure 2.2 shows a picture of the current reactor used for the experiments. The reactor consists of two vertical channels of rectangular cross sections that are positioned opposite to each other. The rectangular channels have an aspect ratio of about 10, which make one horizontal dimension (y-axis, shorter side) negligible, and thus nanoparticles produced can evolve only along the z direction. In one of the channels nitrogen plus hydrogen gas mixture is flowing and on the other side nitrogen plus oxygen is input. The two streams impinging on each other form a stagnation plane with a location defined by the ratio of the momentum of the two streams; for example, equal momentum means a stagnation plane in the middle between the two nozzles. The stagnation plane is in good approximation flat and the radial component of the velocity is always positive (that is no gas is flowing back towards the center).

The precursor is input in the stream mixture N_2+H_2 and carried up to the flame. A probe holding a TEM grid is shot into the flame to collect nanoparticles with a two-way pneumatic valve that allows rapid insertion and retraction of the probe in about 60 milliseconds each way. Each sample was later observed under the TEM. The TEM images were analyzed to obtain the particle size distribution.

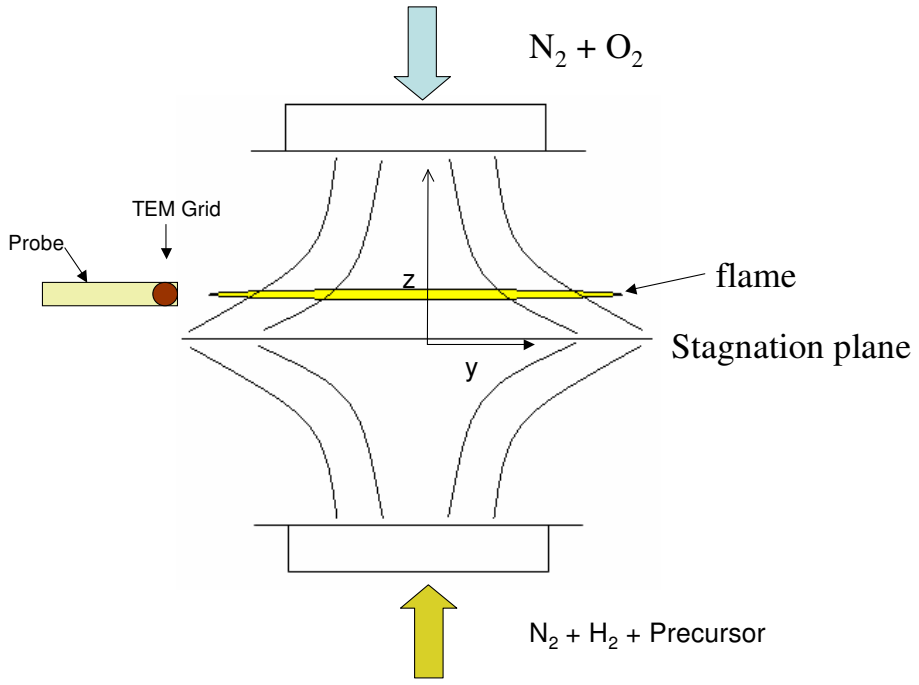

Figure 2.1. Schematic representation of the CDF reactor.

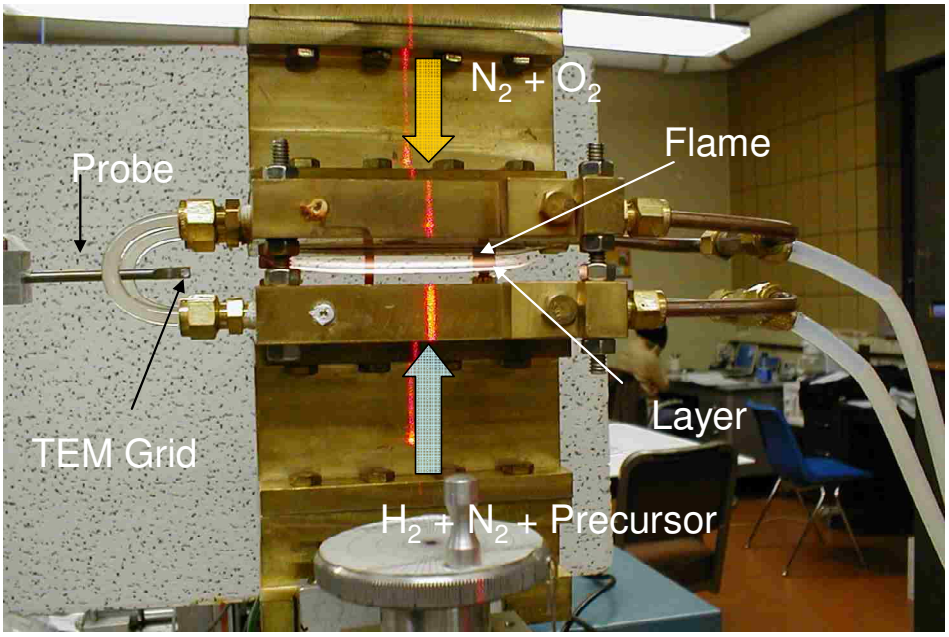

Figure 2.2. CFD reactor used for synthesis of nanoparticles.

2.2. EXPERIMENTAL PROCEDURES

2.2.1. Measurements of Flame and Stagnation Layer position. The position of the flame and the stagnation layer were measured as part of the flame structure characterization. For this purpose a telescope measurement system was used. The system consists of a telescope with 5x magnification lens attached to a metal stand and an analog displacement sensor. The metal stand consists of a base with a mil**l**imetric displacememnt screw mechanism that allows setting the vertical position of the telescope. A schematic drawing of the telescope measurement system is show in Figure 2.3. The telescope has a horizontal guideline built into the lens that can be used as visual aid to mark the location height of a give feature. The telescope was coupled to a displacement sensor so that any changes in the telescope height were automatically measured with a precision of 0.001 inch or 0.02554 mm.

The measurements of the flame and stagnation layer were performed as follows: first, the telescope was reset in the horizontal position using a laser level. Then the telescope was vertically moved to the zero position by matching the horizontal line of the telescope view with the lower exit channel in the reactor. The displacement gauge was then reset to zero. Any further vertical displacements of the telescope can be measured relatively to the reactor lower channel exit.

Once the telescope was reset to zero position, measurements of the flame and stagnation layer were taken simply by visually leveling the telescope with the lower and upper limit height of each flame or stagnation layer and recording the height measured in the displacement sensor.

Due to small fluctuations of the gas flow the flame and the stagnation layer position could change slightly from for each measurement. The measurements were taken consecutively at least two times or until obtaining a reproducible reading of the height recorded. The typical standard deviation of reproducible readings was in the range of 1 to 3% of the average readings value.

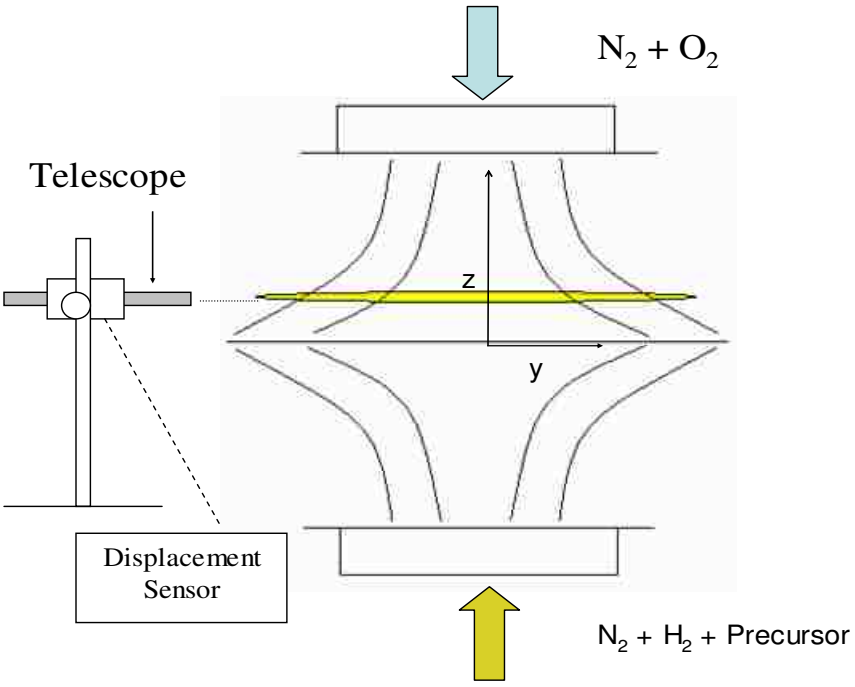

Figure 2.3. Schematic drawing of the telescope measurement system.

2.2.2. Calculation of mv ratio and equivalence ratio. The characterization of the synthesis conditions requires the calculation of the momentum ratio as well as the equivalence ratio.

The momentum ratio is calculated as follows: first the average gas flowing velocity was calculated using the gas flow rate and the area at the each channel exit. For example, assuming a gas flow rate of H_2 equal to 2.86 l/min, and the channel exit area (A) equal to 6 cm^2, then the average velocity at the channel exit for this gas will be equal to the area A multiplied by the gas flow rate, that is:

2.86 [l/min] * 1000 [cm^3]/1[l] /6 [cm^2] = 492.85 [cm/min] or 0.0821 [m/sec]

The same calculation of the average gas velocity is done for each gas flow rate; thus the momentum ratio for the given gas flow conditions at the exit of the channel reactor can be calculated. Table 2.1 summarizes the average velocity for each gas flow

rate. The momentum ratio of the inlet flow in the hydrogen side is then the sum of the gas momentum in the hydrogen side divided by the sum of momentum for the oxygen side. Table 2.2 shows the momentum ratios calculated for the gas flow rate conditions from table 2.1.

With respect to the equivalence ratio, this parameter is defined as the ratio between the molar ratio for stoichiometric combustion and the molar ratio for the gas conditions at the entrance of the reactor channels. The combustion reaction of hydrogen and oxygen can be written as follows:

$$H_2 + ½\ O_2 => H_2O \qquad (3)$$

From equation (3) 1 mol of H_2 are required for every 0.5 mol of O_2, thus stoichiometric molar ratio of hydrogen to oxygen is then equal to 2. From table 2.2 the actual molar ratio of the gas conditions is:

$$(0.00224\ [\text{mol of } H_2/\text{s}])/(0.00149\ [\text{mol of } O_2/\text{s}]) = 1.5$$

The equivalence ratio is then equal to 1.5 /2 = 0.75

Table 2.1. Gas flow rate and average velocity for a given flame condition

			Average Velocity [m/s]	
Gas	Volumetric Flow rate [l/min]	Area [cm^2]	Upper Channel	Lower Channel
O_2	1.97	6	0.0548	-
N_2/O_2	2.25	6	0.0624	-
N_2/H_2	1.92	6	-	0.0535
H_2	2.96	6	-	0.0821

Table 2.2. Momentum (mv), Momentum ratio (mv ratio) and equivalence ratio for the gas conditions show in table 2.1

			Average momentum mv [mol*m/s^2]				
Gas	Volumetric Flow rate [l/min]	MW [g/mol]	Upper Channel	Lower Channel	mv ratio	Molar flow rate [mol/s]	equivalence ratio
O_2	1.97	32	8.18E-05	-		0.00149	
N_2/O_2	2.25	14	1.06E-04	-	1.392602	0.00170	0.75
N_2/H_2	1.92	14	-	7.80E-05		0.00146	
H_2	2.96	2	-	1.84E-04		0.00224	

2.2.3. Nanoparticle sampling procedures. The procedures to obtain a nanoparticle sample from a given flame conditions can be summarized into two methods: direct probe collection and a dry vacuum collection method.

In the probe sampling method a probe was used to obtain the sample. The probe was attached to a pneumatic piston that shoots the probe into the flame at a high speed. The probe tip has attached a TEM grid. The nanoparticles are attached to the grid by thermophoresis effect. Typical shooting time was 60 milliseconds. Each grid can sample a height of 3 mm inside the flame structure. Thus for sampling length larger than 3 mm it two or more grids was attached to the probe tip and placed consecutively in height.

With respect to the dry vacuum collection method, this method was used for the experiments performed with the nanocollector. The method to obtain a sample was simply by using a nanocollector system with vacuum. The nanoparticles formed in the reactor are extracted by means of the vacuum pump. A dry filter retains the nanoparticles to form a nanoparticle cake that was eventually take off the filter. Once the sample was collected, the nanoparticles were examined in the TEM. To prepare for TEM samples, a small amount (~0.001 g) of the particles collected from the filter were suspended in 1-propanol alcohol. A drop of the suspension was then placed on a TEM grid and let dry.

2.2.4. Measurements of particle size distribution. The particle size distribution measured from the TEM images obtained from the samples, using digital image processing software (Image Scion version 4.02B). For this purpose the TEM images were scanned and digitalized. The software allows setting the scale from the magnification bar in the digitalized TEM image. For example, at magnification of 69Kx, the bar length (13.5 mm) in the TEM image correspond to a scale of 195.65 nm. Individual particle size was then measured from at number of particles in the range of 70 to 150 particles, depending on the scale and size of the particles. Measurements of particle size distribution were repeated for a given sample using three or more TEM images, assuring in this way a reproducible measurements of particle size were obtained.

3. RESULTS AND DISCUSSION

3.1. FLAME TEMPERATURE MEASUREMENTS

The flame's temperature profile was characterized using direct temperature measurements from thermocouples. First it was determined the corrections required in the temperature measurements due to radiation based on the method of probe thermometry. Figure 3.1 shows the estimated gas temperature profile using bare thermocouples Pt-13%Rd with beads diameters 0.005, 0.015 and 0.025 in. The bead diameters were measured by optical microscopy.

The method to calibrate the thermocouple's radiation effect consists of measuring the temperature profile with several thermocouples bead diameters. As the bead diameter decreases, the effect of radiation in the temperature measurement decreases. Plotting the temperature data for the different bead diameters can be obtained by extrapolation to obtain the true gas temperature.

In Figure 3.1 the maximum gas temperature extrapolated from the results was around 1684 ˚C. This temperature is about 1 % above the value of 1662 ˚C using a thermocouple with 0.005 in bead diameter. Also the maximum gas temperature calculated is 9.5% above the value of 1501 ˚C obtained using a thermocouple with 0.025 in bead diameter. Thus from the data from Figure 3.1 a set of corrections factors can be obtained and used to account for radiation.

In summary, Figure 3.1 shows the correction to obtain the true gas temperature using Pt-13%Rh thermocouples is in the order of 1 to 10 % depending on the bead diameter. The smallest bead diameter (0.005 in) thermocouple was selected to characterize the flame's temperature profile, taking advantage of the smaller correction required to account for radiation among the different diameters tested.

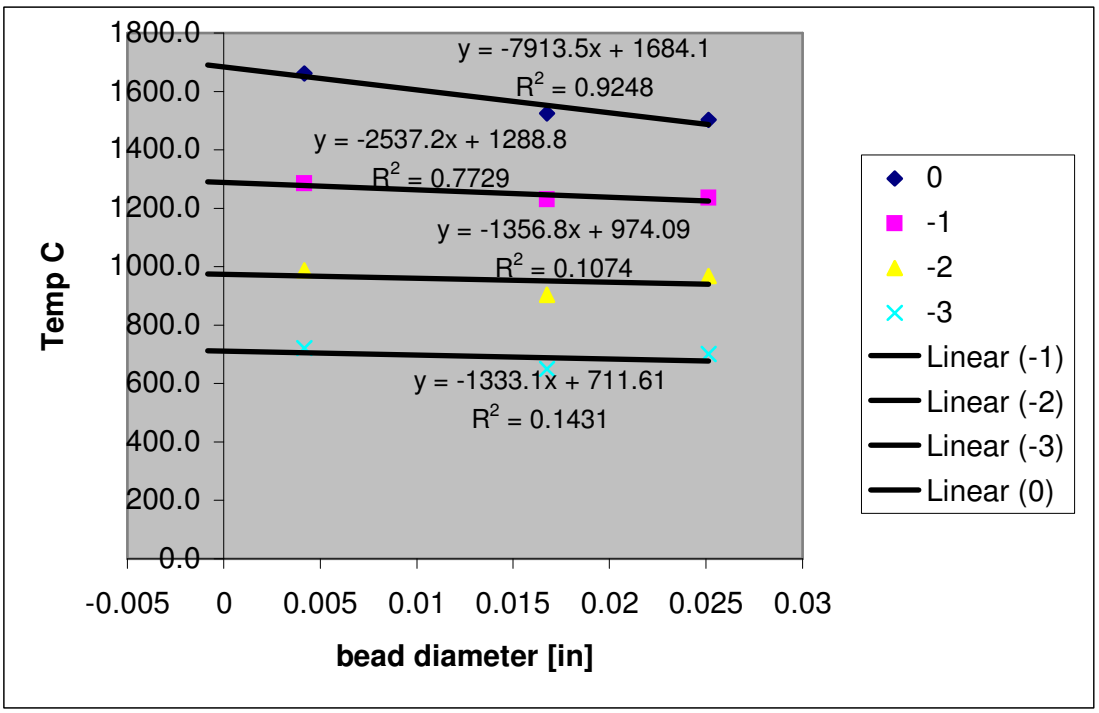

Figure 3.1. Measured gas temperature as function of the thermocouple bead diameter. The numbers in the legend correspond to the distance [mm] from the upper limit of the flame. Hydrogen flow rate 2.42 L/min

Figure 3.2 shows the temperature profiles for two flames, both flames with gas composition are shown in Tables 3.1 and 3.2. The temperature data in Figure 3.2 was obtained using Pt-13%Rh thermocouples 0.005 in diameter and the data compensated for radiation using the data from Figure 3.1. The maximum temperature range for Pt-13%Rh thermocouples is around 1700ºC, so a trend line was calculated based on the data available as well as the correlation factor R^2 to account for accuracy of the trend line.

The momentum ratio (mv ratio) was calculated in the tables as the ratio of the momentum of hydrogen stream to the momentum of the oxygen stream. Also the equivalence ratio was calculated as the ratio of the actual molar ratio of hydrogen to oxygen to the stoichiometric molar ratio of hydrogen to oxygen for complete combustion.

Flame (a) has a momentum ratio of 0.435 and equivalence ratio 0.614 (see Table 3.1 and Figure 3.2 a, red line). The second flame shows higher momentum ratio of 1.853 and lower equivalence ratio 0.460 (see Table 3.2 and Figure 3.2 a, green line).

Comparing gas conditions (see Tables 3.1, 3.2) Flame (a) corresponds to a lower gas velocity than Flame (b) but the momentum ratio is about 3.6 times higher. These conditions mean longer residence time in the case of Flame (a). On the other hand, equivalence ratio for both Flames is less than 1, with flame (a) equivalence ratio 1.33 times higher than flame (b). Thus flame conditions in Flame (a) are more reducing compared with Flame (b) (see Tables 3.1 and 3.2). Also it can be observed that the flame with higher equivalence ratio (flame (a) in Figure 3.2) has the lowest momentum ratio. Particles in flame (a) will experience lower velocities, that is, longer residence time as well as overall lower temperatures compared to flame (b). On the other hand, particles in flame (b) will experience higher temperatures and shorter residence times.

The combination of momentum ratio and temperature profile controls the heating rate that particles will experience moving toward the flame. As seen in Figure 3.2, the temperature rate changes in both the hydrogen side and oxygen side as gas flow rate increases. It can be observed that as hydrogen flow rate increases, it displaces the flame upward; basically there is a displacement of the flame position because of higher gas velocity. Considering the temperature profile in Figure 3.2 and the average gas velocity in Table 3.1 and 3.2, it is is estimated a heating rate of 96×10^3 °F/s in flame (a) compared

with $32x10^3$ °F/s in flame (b). Particles will experience higher heating rates when they will approach to the flames in flame (a) than in the case of flame (b).

In summary, it can be concluded that the temperature profile and environment that particles experience is controlled by multiple parameters. Thus the nanoparticle evolution in the flame not only depends on the temperature profile but also on the momentum ratio and equivalence ratio.

The results in section 3.1 show that the temperature profile can be controlled in the flame by variations of hydrogen flow rate maintaining all other conditions constant. For example, a particle that travels at low hydrogen flow rate will observe higher heating rate, lower maximum temperature (inside the flame), and longer residence times. As hydrogen flow rate increases, nanoparticles formed will observe lower heating rate, higher maximum temperatures (inside the flame), and shorter residence time.

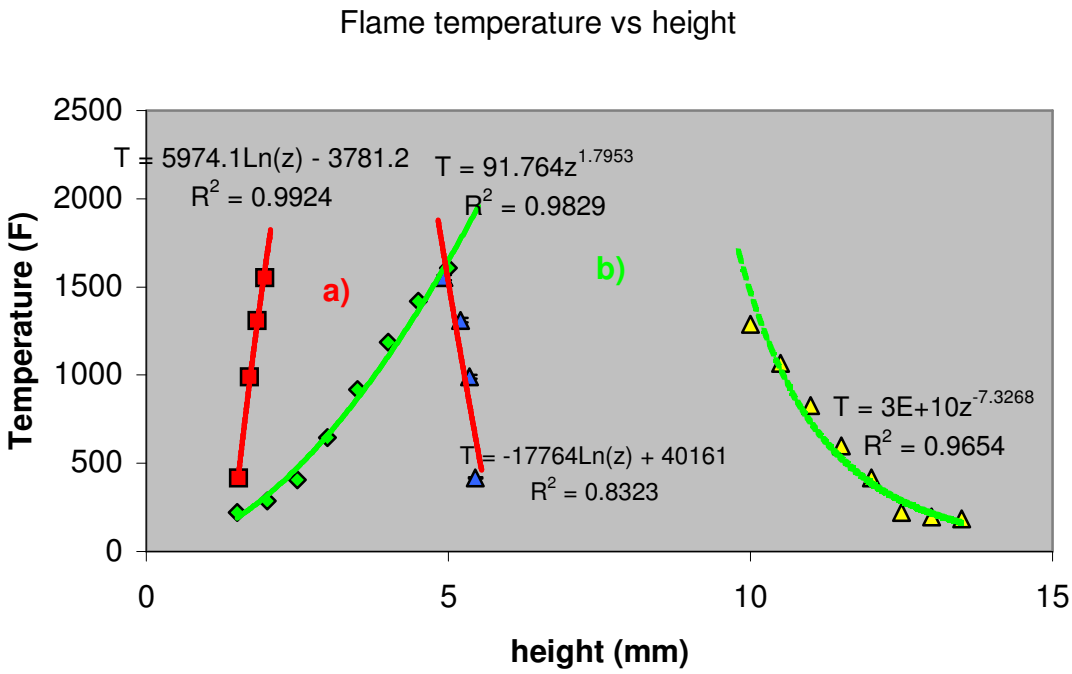

Figure 3.2. Typical flame temperature profiles for two flames. X-Axis represents the height (z) from the bottom channel at which temperature (in ºF) was measured. a) Flame (a): red line with red squares below the flame and red line with blue triangles above the flame. b) Flame (b) green line with green squares below the flame and green line with yellow triangles above the flame

.

Table 3.1 Gas flow rate and stream conditions for a low flow rate flame (Flame a)

		Channel Average Velocity m/s			
Gas	**l/min**	**Upper**	**Lower**	**mv ratio**	**equivalence ratio**
O_2	2.0	0.0329	-		
N_2/O_2	2.2	0.0375	-	0.435	0.614
N_2/H_2	1.9	-	0.0321		
H_2	2.4	-	0.0403		

Table 3.2 Gas flow rate and stream conditions for a high flow rate flame (Flame b)

		Channel Average Velocity m/s			
Gas	**l/min**	**Upper**	**Lower**	**mv ratio**	**equivalence ratio**
O_2	3.4	0.0567	-		
N_2/O_2	3.1	0.0515	-	1.853	0.460
N_2/H_2	6.4	-	0.1073		
H_2	3.1	-	0.0521		

3.2. FLAME STRUCTURE AND NANOPARTICLES EVOLUTION IN THE COUNTERFLOW DIFFUSION FLAME (CDF) REACTOR

In the counterflow diffusion flame, the flame structure is strongly linked with the fluid dynamics established in the opposed jet burners of the flame. In the previous section the flow pattern and temperature profile were characterized for two typical flames, Flame a and Flame b.

The present section will characterize the flame structure and the nanoparticle evolution in the flames. The flame structure at stable gas and precursor flow rates can be described by dividing the flame structure in three characteristic zones starting from the bottom side and upward as follows (see Figure 3.3):

- **Stagnation layer**: zone below the flame where equal momentum of the two streams exist, forming a stagnation plane. A layer is formed in this zone due the precursor decomposition and formation of nanoparticles.
- **Flame**: area where hydrogen and oxygen react forming the combustion zone. Hydrogen posses the lowest density and higher diffusivity and as result it will diffuse faster compared with other gases, so the position of the flame depends mainly on the hydrogen flow rate. The higher diffusivity of hydrogen is also the reason why the flame is usually found above the stagnation plane. Without precursor the flame present a characteristic blue color. When particles are forming from the precursor decomposition the flame is a characteristic yellowish color due to precursor decomposition and particles formation.
- **Top layer**: area above the flame where particles get cooled down after passed through the flame.). Not always the top layer was formed. Only when the stagnation layer is close enough to the flame was observed the formation of this layer. It may also require a precursor rate high enough in the flame. If present, this layer shows a yellowish color due to particle radiation.

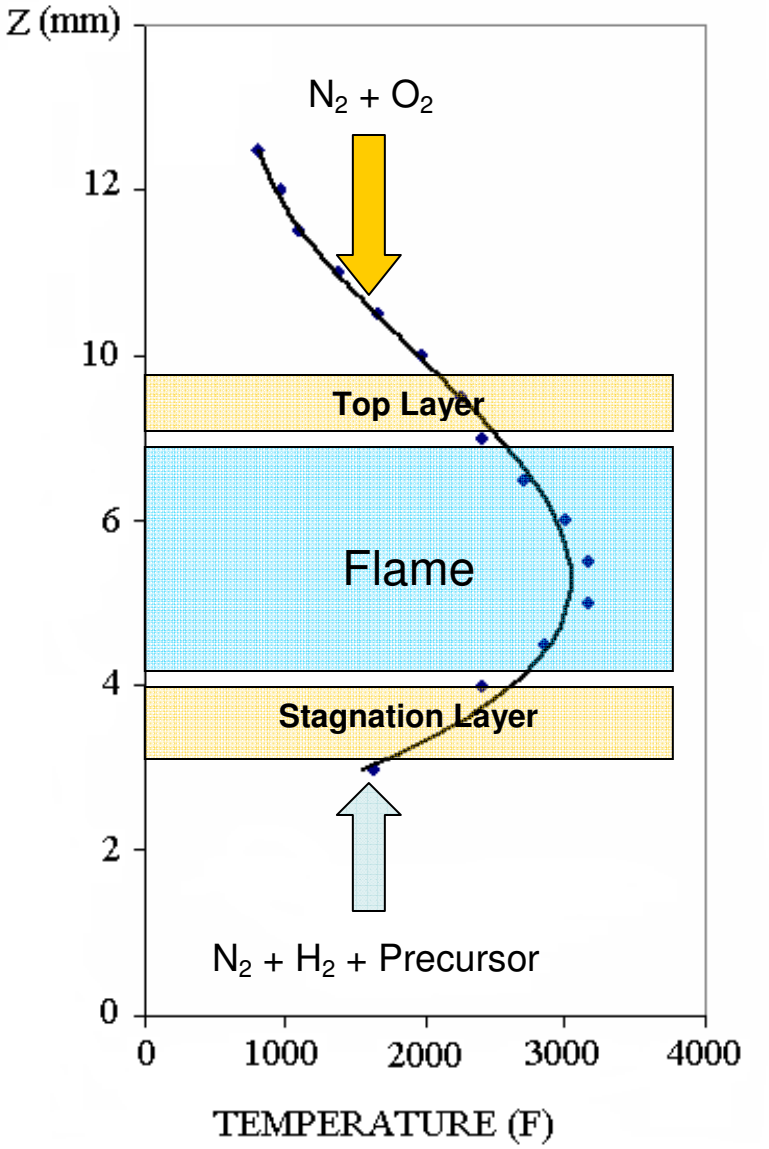

Figure 3.3. Schematic representation of a typical flame's temperature profile and flame structure.

In order to characterize the nanoparticle formation and evolution, Figure 3.4 shows the TEM images of the iron oxide nanoparticles as function of the position in the stagnation layer and flame.

First, at the stagnation layer, the precursor is decomposed due to the rapid temperature increases. Initially agglomerates are formed (Figure 3.4a) and transported toward the flame where they collapse and sinter into single nanoparticles partially or fully (Figure 3.4 b to d), depending on flame and temperature profile conditions. Typically particles found in upper part of the stagnation can vary from hexagonal or spherical, cubic/rectangular and triangular particles.

At the zone between the upper limit of the stagnation layer and the flame level or above (Figure 3.4 d and e) further particle growth occurs and particles are completely crystallized. In the particular sample shown in Figure 3.4 mainly sphere-shape nanoparticles have been found in this zone. Agglomerates and sinters formed previously are destroyed and mostly single nanoparticles can be found in this zone. The final particle size in Figure 3.4 d is about 50 nm.

Also in Figure 3.4 it is noticeable that the density of nanoparticles increases, as they get closer to the flame (see Figure 3.4 d, e). This phenomenon is typically observed when the stagnation zone is close to the fame as previously described in section 3.1. The momentum ratio (mv) for this flame is shown in table 3.1. This value is relative low, and thus the particles will observe lower gas velocities and longer residence time. The stagnation layer is formed close to the flame and the upper part is superimposed with the flame as described in section 3.1. Nanoparticles that traveled faster from the bottom are slowing down in the stagnation layer, thus increasing the density of particles. As residence time is larger at the stagnation layer, particle growth is allowed in this zone. The particles obtained are about 50 nm as shown in Figure 3.4d.

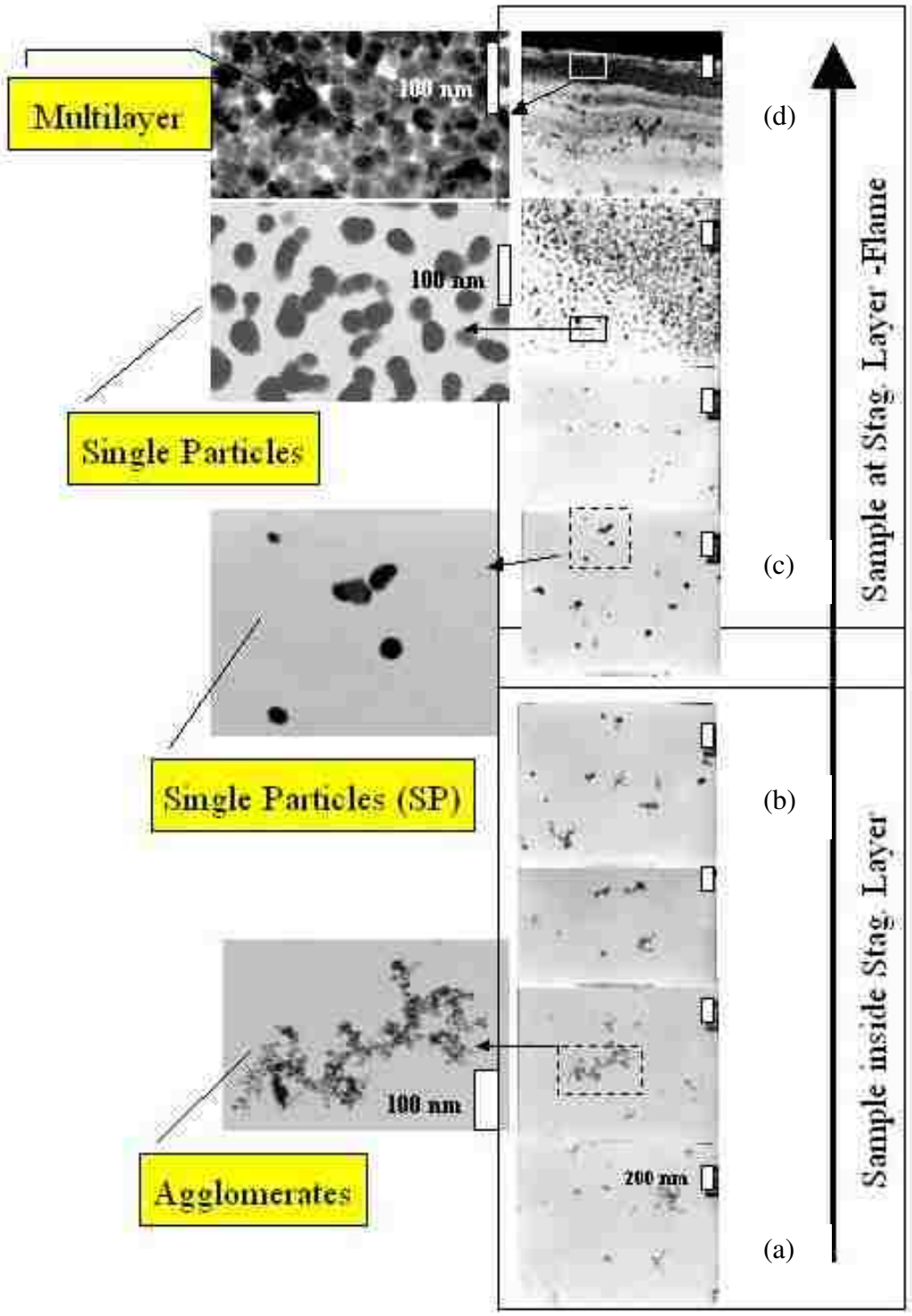

Figure 3.4. Typical nanoparticle formation sequence in a CDF Flame. a) Decomposition of precursor and agglomerates formation. b) and c) Nanoparticles formed from agglomerate. d) Single particles build-up and grow near flame.

3.3. EFFECT OF THE PRECURSOR RATE.

In order to characterize the effect of the precursor rate, Figure 3.5 shows the variation of both flame and stagnation layer positions as a function of precursor feeding rates. Table 3.3 shows the gas flow conditions. The positions of the upper and lower limits in height in the flame and stagnation layer were recorded, taking as a reference of the lower channel plane of the reactor.

In Figure 3.5 it can be observed that the higher the precursor rate, the wider the stagnation layer formed. Both of the positions limit in the stagnation layer and the flame changes when precursor rate increases. The lower limit of the stagnation layer slightly decreases. This lower limit indicates the beginning of the precursor decomposition and formation of agglomerates, also the upper limit of the stagnation layer increases. In contrast in the flame only the lower limit height changes. The lower limit height in the flame increases, as the precursor rate increases. It has been reported in the literature [11] that $Fe(CO)_5$ compounds at low concentration are effective flame inhibitors. The present results corroborate that the flame lower limit is affected by the precursor decomposition.

Figure 3.6 shows the TEM images of iron oxide nanoparticles formed at increasing precursor rates. The TEM images show the particles found at the upper level of the stagnation layer. As expected, the increment of precursor rate produces the formation of bigger average particle size. The sizes of the particles found for the particular set of experiments in Figure 3.6 ranges from around 5 nm (Figure 3.6 a) up to about 70 nm (Figure 3.6c). The shape of the particles is predominantly hexagonal for Figure 3.6, with some degree of nanoparticles agglomeration at higher precursor rates, indicating that increasing the precursor rate mainly affects the particle size obtained. It can also be observed the presence of two size modes in Figure 3.6 b and c.

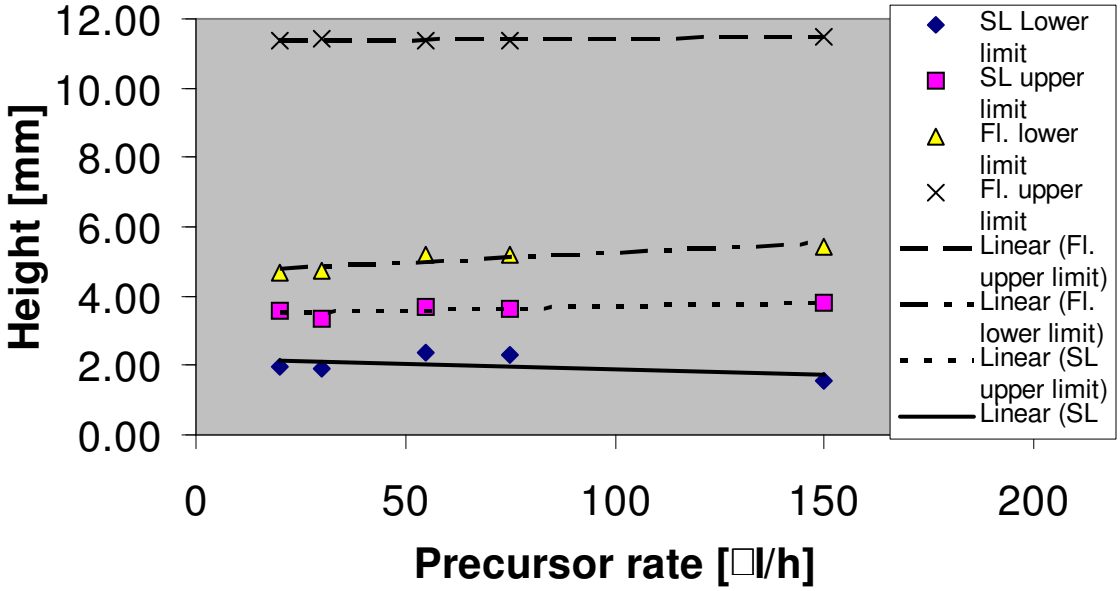

Figure 3.5. Variation of Flame and layers position as function of precursor rate. Abbreviations: SL=Stagnation layer, FL=Flame. As the precursor flow rate increases (with all other flame conditions constant) the stagnation layer height increases as well as the flame lower limit. Hydrogen flow rate set constant at 2.62 l/min.

Table 3.3. Gas flow conditions for flame shown in Figure 3.4

		Channel Average Velocity m/s			
Gas	**l/min**	**Upper**	**Lower**	**mv ratio**	**equivalence ratio**
O2	1.97	0.0329	-		
N2/O2	2.25	0.0375	-	0.442	0.664
N2/H2	1.92	-	0.0321		
H2	2.62	-	0.0437		

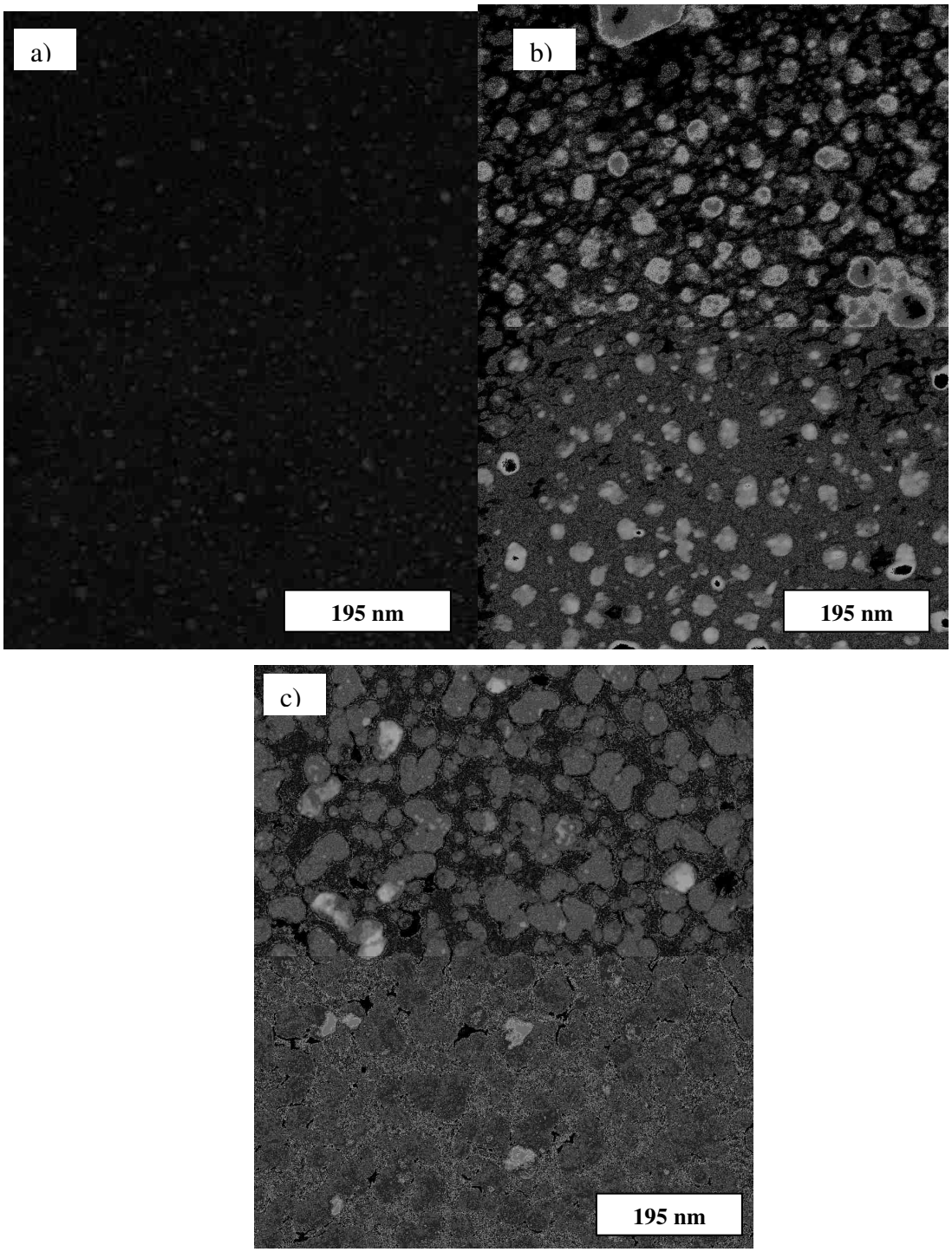

Figure 3.6. TEM images of iron oxide nanoparticles formed at different precursor flow rate. a) 30 µl/h. b) 75 µl/h. c) 150 µl/h.

3.4. HYDROGEN FLOW RATE EFFECT ON THE FLAME STRUCTURE

To characterize the flame structure as a function of hydrogen flow rates, Figure 3.7 shows the flame positions as a function of hydrogen flow rates. The data recorded in Figure 3.7 was the height of the lower upper limit of the stagnation layer, the height of flame lower limit, and the top layer upper limit position as function of hydrogen flow rate. The first observation is that the top layer is formed only at the beginning of the graph where comparatively low hydrogen flow rates conditions are present. In table 3.4, the momentum ratio increases as hydrogen flow rate increases. This means that the position of the stagnation plane is initially set below the middle plane of the reactor and moves upward as hydrogen flow rate increases. For momentum ratio (mv ratio) values around 1, it is expected that the stagnation plane will form around the middle plane between the two channels in the CDF reactor, i.e. about a height of 7.5 mm. For momentum ratios lower than 1, the stagnation plane is formed closer to the hydrogen side. The lower limit of the flame at low hydrogen flow rate is about 6 mm, thus the upper part of the stagnation layer position will overlay the flame at some of the conditions tested. As the stagnation layer is partially inside the flame, then particles can travel trough the flame upward and form a top layer (see Figure 3.7).

As hydrogen flow rate increases, momentum ratio and equivalence ratio also increases and the top layer disappears. The flame forms at higher heights and the stagnation layer does not change its position as the flame does, so the top layer is no longer visible as hydrogen flow rate increases. On the other hand, as equivalence ratio increases, the flame conditions go from oxidizing to reducing conditions. For high hydrogen flow rates the flame's temperature profile is expected to increase.

Table 3.4. Gas flow conditions for flames used in Figure 3.7.

		Average Velocity m/s			
Gas	**l/min**	**Upper**	**Lower**	**mv ratio**	**equivalence ratio**
O2	1.97	0.0329	-		
N2/O2	2.25	0.0375	-		
N2/H2	1.92	-	0.0321		
H2	4.54	-	0.0757	0.547	1.15
	4.19	-	0.0698	0.524	1.06
	3.84	-	0.0640	0.502	0.97
	3.48	-	0.0581	0.482	0.88
	3.31	-	0.0551	0.473	0.84
	3.13	-	0.0522	0.465	0.79
	2.95	-	0.0492	0.456	0.75
	2.78	-	0.0463	0.449	0.70
	2.60	-	0.0433	0.442	0.66
	2.42	-	0.0404	0.435	0.61
	2.24	-	0.0374	0.429	0.57
	2.07	-	0.0345	0.423	0.52

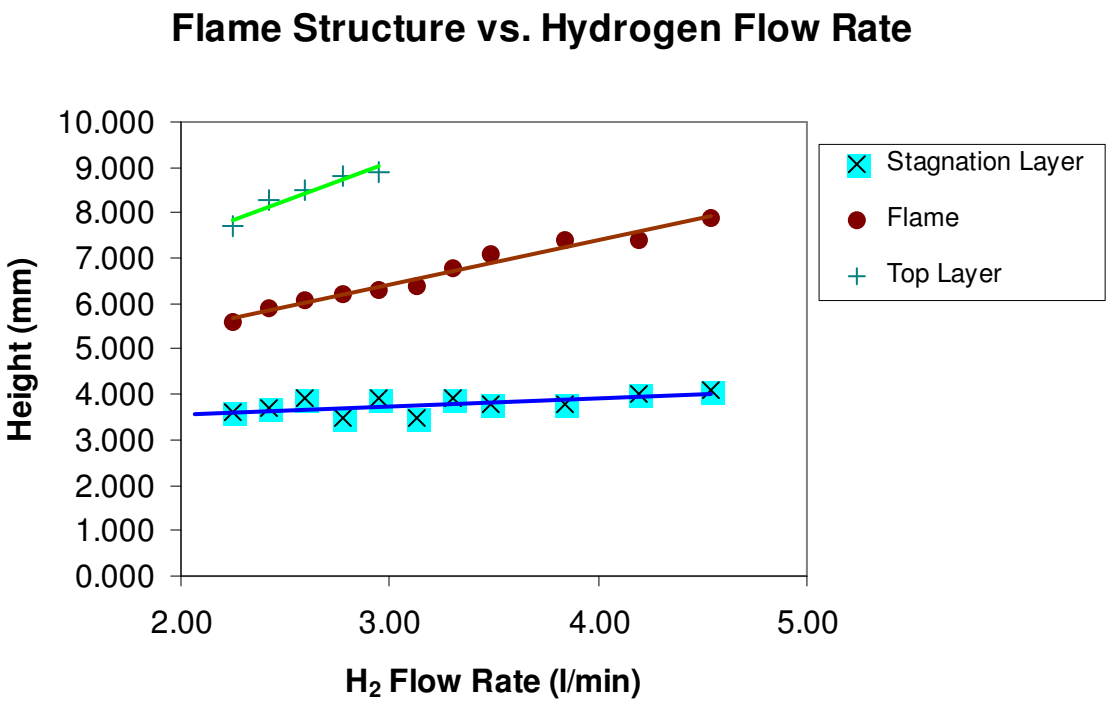

Figure 3.7 Variation of flame lower limit, stagnation layer lower limit and top layer upper limit as function of hydrogen flow rate.

In summary, the evolution of iron nanoparticles in the flame was characterized. It was identified that the formation of agglomerates was at the beginning of the stagnation layer, followed by the collapse of such agglomerates. The final evolution step is the formation of single nanoparticles at higher positions in the stagnation layer.

The flame structure in the CDF reactor presented three characteristics zones. The effect of variation in the precursor flow rate (Figure 3.5) shows that the lower limit of the flame is increased as the stagnation zone increases in width. Also the variation of precursor rate increases the average particle size. The effect of increasing hydrogen flow rates (Figure 3.7) is comparatively larger with respect to the variations of precursor flow rate. Hydrogen flow rate increases the momentum ratio in the flame as well as the temperature profile. Under some conditions it is possible that the upper part of stagnation zone overlay with the flame position and a top layer above the flame is formed.

3.5. DESIGN OF EXPERIMENTS (DOE) FOR VARIATIONS IN SYNTHESIS CONDITIONS VS. NANOPARTICLE SHAPE:

In order to correlate the effect of variation of synthesis conditions with percentage of a given shape of nanoparticles produced, a design of experiments (DOE) was performed. The DOE consisted of a Taguchi Design (L16, with 2 factors of 4 levels, and 3 factors of 2 levels as indicated in Table 3.5). The Taguchi Parameter Design approach attempts to find the optimal levels for the factors studied. The design models the results by using the analysis of means, which give quantitative information on the control factor effects.

The main goal of the study was to find out which of the factors that set the flame conditions will be more effective as a control factor for the synthesis of a given particle shape. It is important to understand that even though the formation of the nanoparticles evolves following the temperature profile explained in section 3.2, the DOE study in the present section was aimed to correlate systematical variations of the flame parameters that maximize production of single nanoparticles of a given shape.

For each experiment in the DOE-1 (table 3.5), a sample was obtained by shooting the probe with a TEM grid into the flame. The position of the probe with respect to the flame was recorded as well as the flame conditions. Duplicated samples were obtained to account for reproducibility of the results. The samples were observed in the TEM and the percentages for each type of particles, namely: cubic, spherical or hexagonal nanoparticles were calculated from these images. The Taguchi DOE allows obtaining the main effect plot for means and contour plot for the percentage cubic particles, and they are shown in Figures 3.8 and 3.9. For hexagonal nanoparticles the respective set of plots are shown in Figure 3.10 and 3.11.

.

Table 3.5 Description of factors and levels used

Factor	Description / levels
H_2 [l/min]	Flow rate of H_2 in L/min, Levels: 2.42 (0.60 reading), 2.95 (0.75 reading), 3.66 (0.95 reading), 4.37 (1.15 reading)
ProbeT °C	Temperature of the probe in Celsius degree, Levels: -20 (Cooled with Dry liq. N_2), 100, 200, 400
PrecRate	Precursor pumping rate (µl/h); Levels: 500, 800 (corresponding to a % Vol of 0.043% and 0.069%)
ProbeP	Probe position, Levels: Probe at top layer (Top), Probe at bottom layer (Bottom)
FlameConf	Flame configuration; Levels: H2Top (H_2 inflow at top of reactor), H2Bottom (H_2 inflow at Bottom of reactor)

Note: Used one-channel reactor with O_2 and N_2/O_2, N_2/H_2 flow rates were set constant for all the experiments at equal to 1.97, 2.25 and 1.92 l/min respectively (see table 3.6).

Table 3.6 Gas flow conditions for flames in DOE-1

		Average Velocity m/s			
Gas	**l/min**	**upper**	**lower**	**mv ratio**	**equivalence ratio**
O_2	1.97	0.0016	-	-	-
N_2/O_2	2.25	0.0009	-	-	-
N_2/H_2	1.92	-	0.0007	-	-
H_2	4.37	-	0.0005	0.5352	1.1078
	3.66	-	0.0003	0.4920	0.9283
	2.95	-	0.0002	0.4565	0.7488
	2.42	-	0.0001	0.4348	0.6142

3.5.1. Synthesis Conditions for cubic-shape nanoparticles. The experimental results for the synthesis conditions of cubic-shape nanoparticles are shown in Figure 3.8 and 3.9. The data in Figure 3.8 was also used to represent the corresponding contour plot of percentage of cubic nanoparticles as function of flow of H_2 and Probe temperature in Figure 3.9.

The main effect plot for the hydrogen flow rate factor (Figure 3.8) suggests that for the range of conditions tested, there is a minimum amount of cubic nanoparticles. When synthesis was performed at H_2 flow rate levels between 2.95 and 3.66 l/min no cubic nanoparticles were observed. At hydrogen flow rate lower or higher than this range, the percentage of cubic particles increases. A possible explanation for this behavior can be found by analyzing the chemical stoichiometric balance and temperatures in the flame. Oxygen flow rate was set constant for all the experiments and equal to 1.97 l/min. To reach stoichiometric conditions in the flame, it requires a hydrogen flow rate of 0.985 l/min. Initial levels of hydrogen flow rate are set for excess of oxygen. As hydrogen flow rates are increased, the flame chemical composition becomes hydrogen richer (see table 3.5), i.e., stronger reducing conditions.

Using as a reference for the discussion about formation of radicals in the flame from Xing et al [9], as H_2 flow rate increases the flame temperature and also stability and concentration of radical's in the flame changes as follows:

- At low hydrogen flow rates (levels 2.42 and 2.95 l/min, Figure 3.8), flame temperatures are comparatively lower, so the stability and abundance of OH and H radicals is lower. Particles formed under these conditions observed both low temperature profile and low radicals stability/concentration.
- As hydrogen flow rate increases, flame positions move upward and temperature profile changes. Radicals became more stable over a large volume in the flame, so particles formed at near stoichiometric conditions has a maximum in both flame temperatures and radicals stability/concentration.
- When excess of hydrogen is present, flame temperatures are no longer proportional to hydrogen flow rate and both temperature and radical's stability decrease.

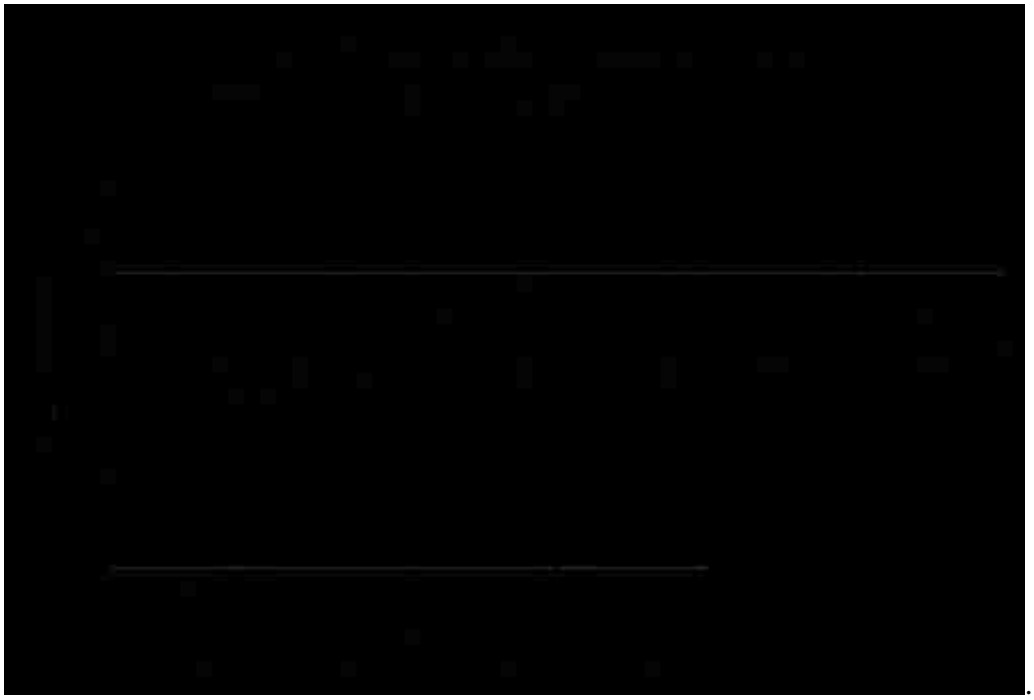

Figure 3.8. Main effects plot for means of % cubic nanoparticles.

From the results in figure 3.8, the effect of the H_2 flow rate is observed with a minimum percentage of cubic nanoparticles found at 3.66 l/min, increasing the amount of cubic nanoparticles at either end of the range tested. Under the near stoichiometric flame conditions and high flame temperatures cubic particles are not formed.

In addition, in Figure 3.8 a max percentage of cubic nanoparticles associated with the probe temperature of 200 °C can be observed. This result points out that the optimum probe temperature for collecting nanoparticles is in that range. Figure 3.9 shows that a maximum percentage of cubic nanoparticles was observed when the probe temperature is around 200 °C. The behavior can be associated to thermophoresis of nanoparticles as reported in the literature [13]. The temperature gradient between the probe surface and the environment containing the nanoparticles (stagnation layer and flame) causes the diffusion of the nanoparticles. These results point out that this thermophoresis effect can be tuned to obtain a maximum amount of collected nanoparticles.

The effects of all other parameters on the percentage of cubic nanoparticles obtained are lesser compared with both H_2 flow rate and probe temperature (Figure 3.8).

The effect of precursor rate can be described as follows: at 500 µl/h the percentage of cubic nanoparticles obtained is greater than at rate of 800 µl/h, that is the increment in precursor rate is inversely proportional to the amount of cubic nanoparticles produced in the flame. This effect only accounts for about 4 % difference in the amount of cubic nanoparticles found.

Placing the probe at the top increases the collection of cubic nanoparticles (see Figure 3.8). This effect is smaller compared with the effect of other factors studied. The flame can be stabilized on either the fuel or oxidizer side of the stagnation plane through suitable dilution of the reactant streams. For most of the conditions tested, the flame was stabilized above the stagnation plane. Thus shooting the probe at the top of the reactor will encounter high temperatures and the increase in temperature promotes the thermophoretic collection of the nanoparticles.

For the flame configuration, placing H_2 gas input at the bottom of the reactor increases the amount of cubic nanoparticles found. Again this effect is smaller compared with the ones observed for hydrogen flow rate and probe temperature. The effect accounts for about 3% differences in the amount of cubic nanoparticles found.

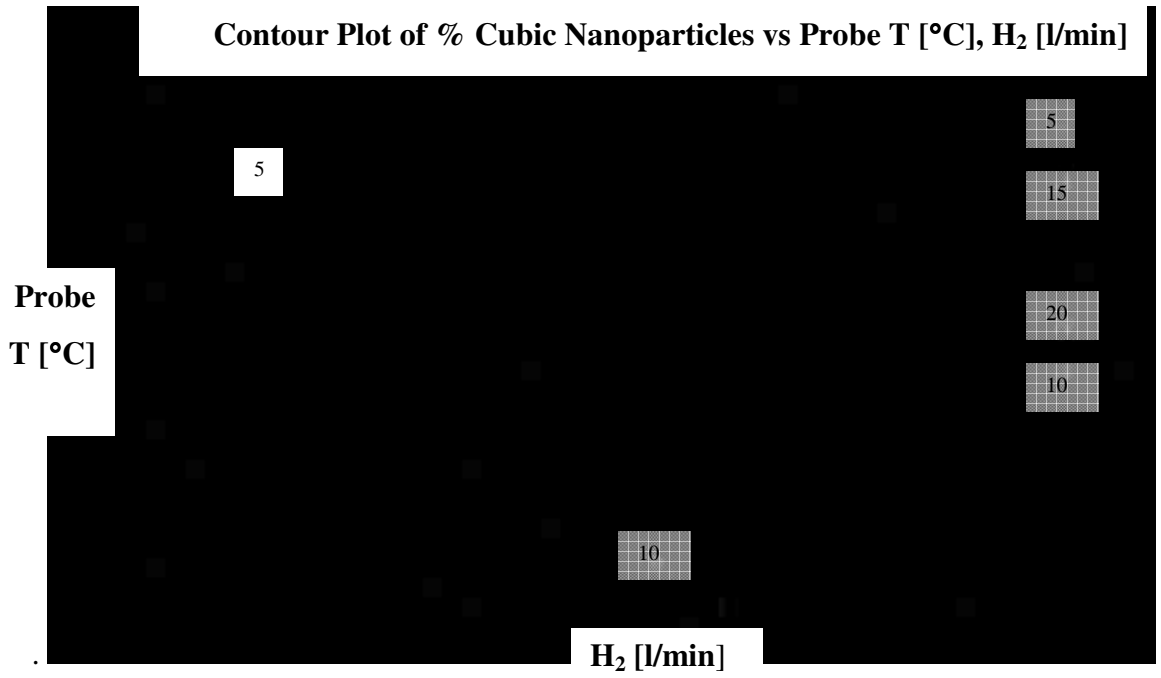

Figure 3.9. Contour plot of the % cubic nanoparticles as function of flow of H_2 and probe temperature. Is observed a region were the amount of cubic nanoparticles increases at higher probe temperature and H_2 flow rate.

3.5.2. Synthesis conditions for hexagonal-shape nanoparticles. The hexagonal shape is the most common shape observed. As in the previous case, hydrogen flow rate is the most important parameter to control the amount of hexagonal nanoparticles. Other parameters, namely, precursor rate, probe position, and flame configuration, have a minor effect on the type of particles obtained. The main effect of each parameter can be discussed as follows.

Hydrogen flow rate: In Figure 3.10, hexagonal-shape nanoparticles are the only particle shapes formed when the hydrogen flow rate is between 2.96 and 3.66 l/min. Figure 3.12b shows a sample of mostly hexagonal nanoparticles at relatively high hydrogen flow rates (2.95 l/.min). As explained before, when the stagnation layer is set close enough to the flame, it overlay the flame. Particles will observe higher temperatures inside the flame before they exit at the upper part of the stagnation layer. As expected the sample is composed only of single hexagonal nanoparticles, without agglomerates between flow rates of 2.96 and 3.66 there is a maximum of hexagonal shape particles formed.

Figure 3.12 shows the TEM image of nanoparticles produced in the flame reactor with different shape distributions. Figure 3.12a shows 90% hexagonal shape and 5% cubic nanoparticles. Figure 3.12b shows > 95 % hexagonal nanoparticles formed on the top layer of the flame reactor.

Probe temperature: This is the second factor in importance in forming hexagonal nanoparticles. The higher the probe temperature, the more hexagonal nanoparticles are found. Thus thermophoresis is an important mechanism to collect nanoparticles that is observed also for the case of cubic nanoparticles. The probe temperature is directly proportional to the amount of hexagonal nanoparticles observed up to a value of 200°C. Again a maximum amount of collected nanoparticles is observed at this temperature. The behavior can be also explained by thermophoresis as previously described for the case of cubic nanoparticles.

Probe position: This parameter have a smaller effect compared with the previous two factors discussed above. Comparing this result with the results for the percentage of cubic nanoparticles, in a similar fashion more hexagonal nanoparticles were also found at

the top of the reactor. Shooting the probe at the top will encounter higher temperatures that eventually increase the thermophoretic effect.

Precursor feeding rate: The effect due to this factor is also smaller compared to the first two factors discussed above. The greater the precursor rate, the lower the percentage of hexagonal nanoparticles. Clearly the higher the precursor rate the less likely that agglomerates decompose and form single nanoparticles.

Flame configuration: This is also in a similar fashion to the results found in the percentage of cubic nanoparticles, locating the hydrogen at the bottom channel of the reactor increases the percentage of hexagonal nanoparticles. The reason for this is that, as stated before, hydrogen is a lighter gas compared to others and will diffuse upward. Thus when hydrogen is located at the top channel of the reactor, it will also diffuse upward and that makes more likely the formation of a higher reducing flame condition in the reactor.

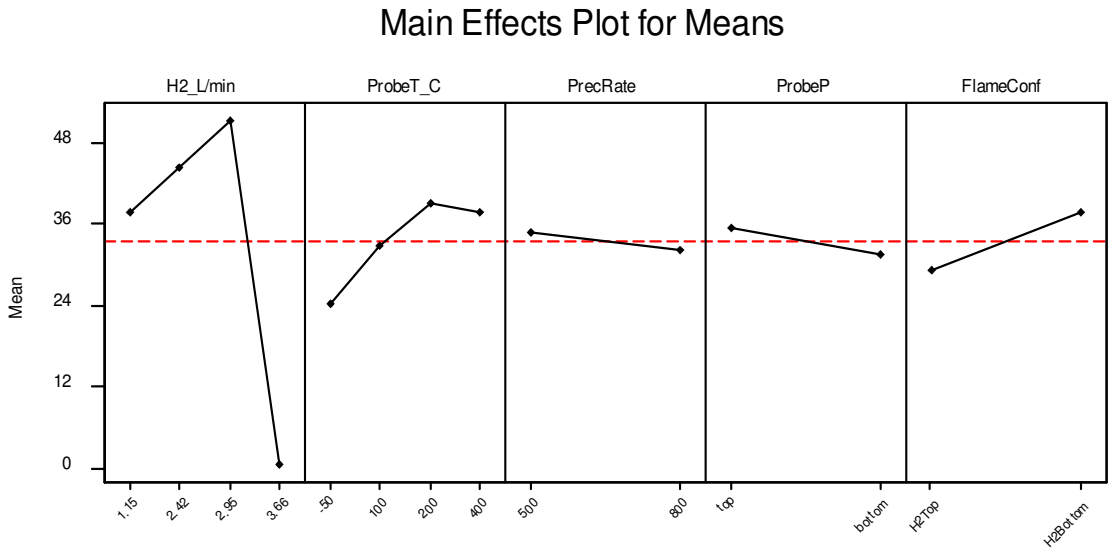

Figure 3.10. Main effects plot for means of % hexagonal nanoparticles.

Figure 3.11 plots the same set of results, this time only correlating the two most significant parameters to control the percentage of hexagonal nanoparticles, namely hydrogen flow rate and the probe temperature. It can be observed that there is a set of conditions where 100 percent of hexagonal nanoparticles are form; corresponding to relatively low hydrogen flow rates and moderate probe temperature at around 200°C.

In summary, among all the parameters studied, the main factors that control the percentages of nanoparticles of a given shape are mainly hydrogen flow rate and the probe temperature. These factors control the temperature profile as well as the effect of thermophoresis. The last can be used to increase collection efficiency and possibly filter out what type of particles that can be collected

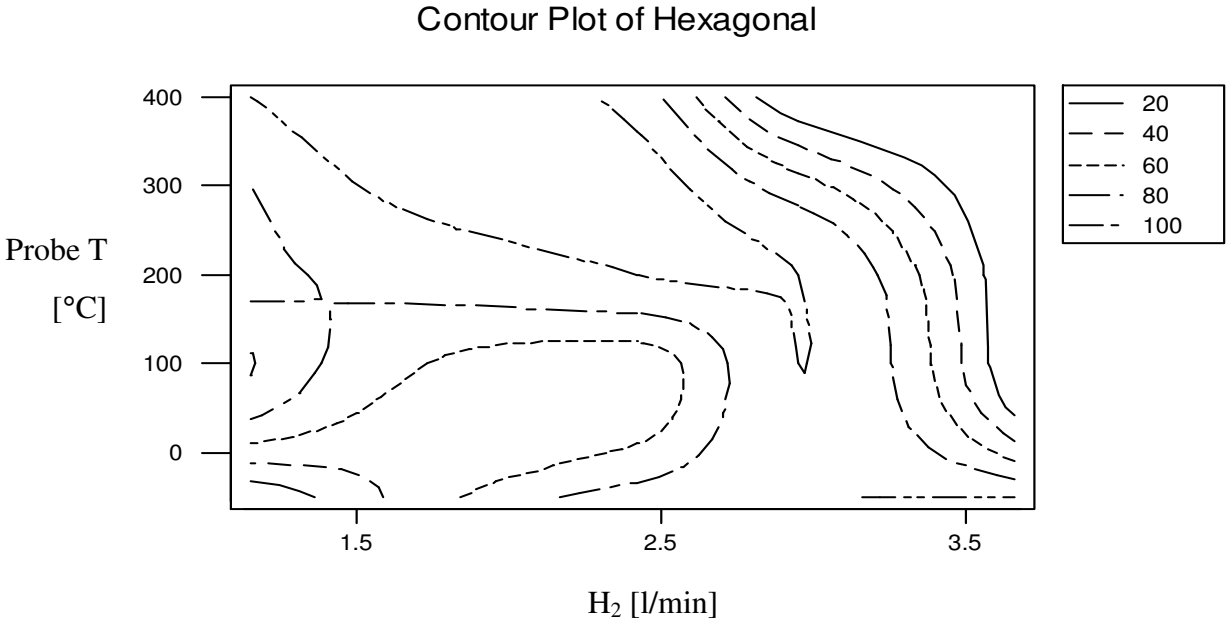

Figure 3.11. Contour plot % hexagonal nanoparticles as function of flow of H_2 and probe temperature. Notice there is a region where 100 % hexagonal particles are obtained at relatively high H_2 flow rates and probe temperature.

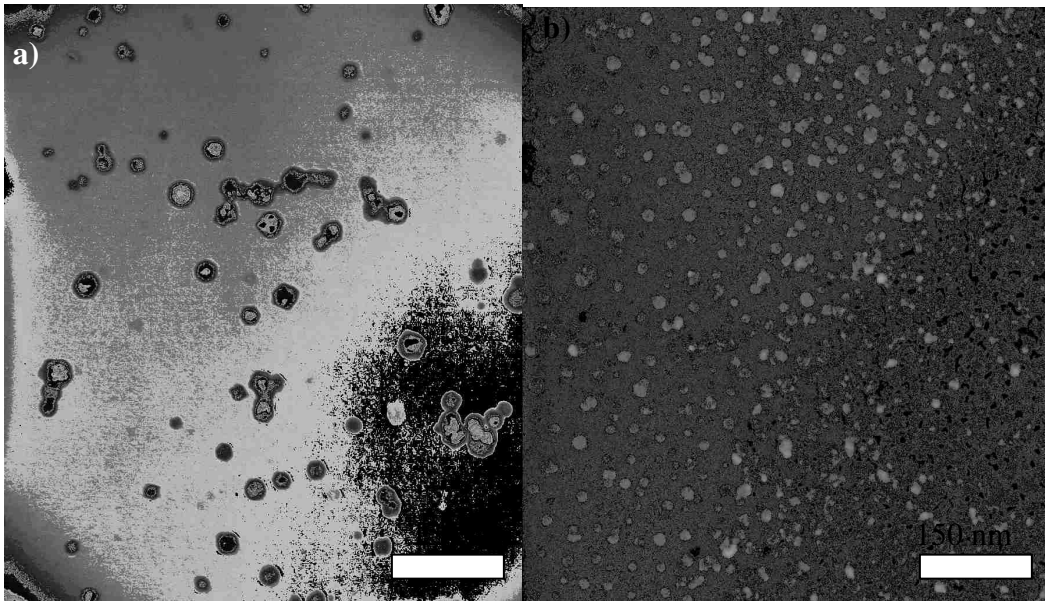

Figure 3.12. TEM image of nanoparticles produced in the flame reactor with magnification at 88.6Kx. a) Shape distribution of nanoparticles formed below the flame. b) Hexagonal nanoparticles formed at high H_2 flow rate on the top layer of the flame reactor.

3.6. DESIGN OF EXPERIMENTS (DOE) FOR VARIATIONS IN SYNTHESIS CONDITIONS USING A NANOPARTICLE COLLECTOR

A method to collect nanoparticles from the flame reactor was designed. The goal was to develop a method to collect nanoparticles directly from the flame in dry conditions. The design of the nanocollector is shown in Figure 3.13 and 3.14. Basically the nanoparticles are collected in a filter holder by using low vacuum conditions in order to minimize disturbance in the flame flow pattern.

The system nanocollector-CDF reactor was set partially closed, that is the system was allowed to flow in some air or flow out excess gases that overcome a given vacuum flow rate. The infiltration air cools down the gas temperature inside the nanocollector and therefore no cooling system was required in the nanocollector. The temperature in the piping that connects the nanocollector with the filter assembly was heat-controlled in the range of 80 to 100 °C using a heating tape.

The gas volumetric balance ($Q_{balance}$) in the nanocollector can be defined as the sum of the volumetric flow rate in the reactor (Q_{cdf}) and the volumetric flow rate from infiltration (Q_{infil}), minus the volumetric flow rate in the vacuum pump (Q_{Vacuum}):

$$Q_{balance} = Q_{cdf} + Q_{infil} - Q_{Vacuum} \tag{2.1}$$

If $Q_{balance}=0$,

$$Q_{cdf} + Q_{infil} = Q_{Vacuum} \tag{2.2}$$

for conditions where $Q_{balance} \neq 0$. The flame flow pattern is distorted in the x-y plane and the flow pattern that nanoparticles follow changes accordingly. Two cases can be described as follows:

$$Q_{balance} < 0 \Rightarrow Q_{cdf} + Q_{infil} < Q_{Vacuum} \text{ (low vacuum condition)} \tag{2.3}$$

$$Q_{balance} > 0 \Rightarrow Q_{cdf} + Q_{infil} < Q_{Vacuum} \text{ (low pressure-differential condition)} \tag{2.4}$$

Ideally the nanoparticle synthesis and collection process should be set to $Q_{balance} = 0$. In reality, the process follows an initial stage where $Q_{balance} < 0$. As the filter is filled up with nanoparticles, the system changes to ideal balance and subsequently to $Q_{balance}>0$, i.e. low differential pressure. In the experimental setup a dry mechanical pump was used where the vacuum level is inversely proportional to the gas flow rate passing through the pump. As vacuum increases, gas pumping rate decreases. Table 3.10 shows the values of each flow rate (Q_{Vacuum},Q_{cdf},Q_{infil}) with Q_{infil} calculated for $Q_{balance}=0$.

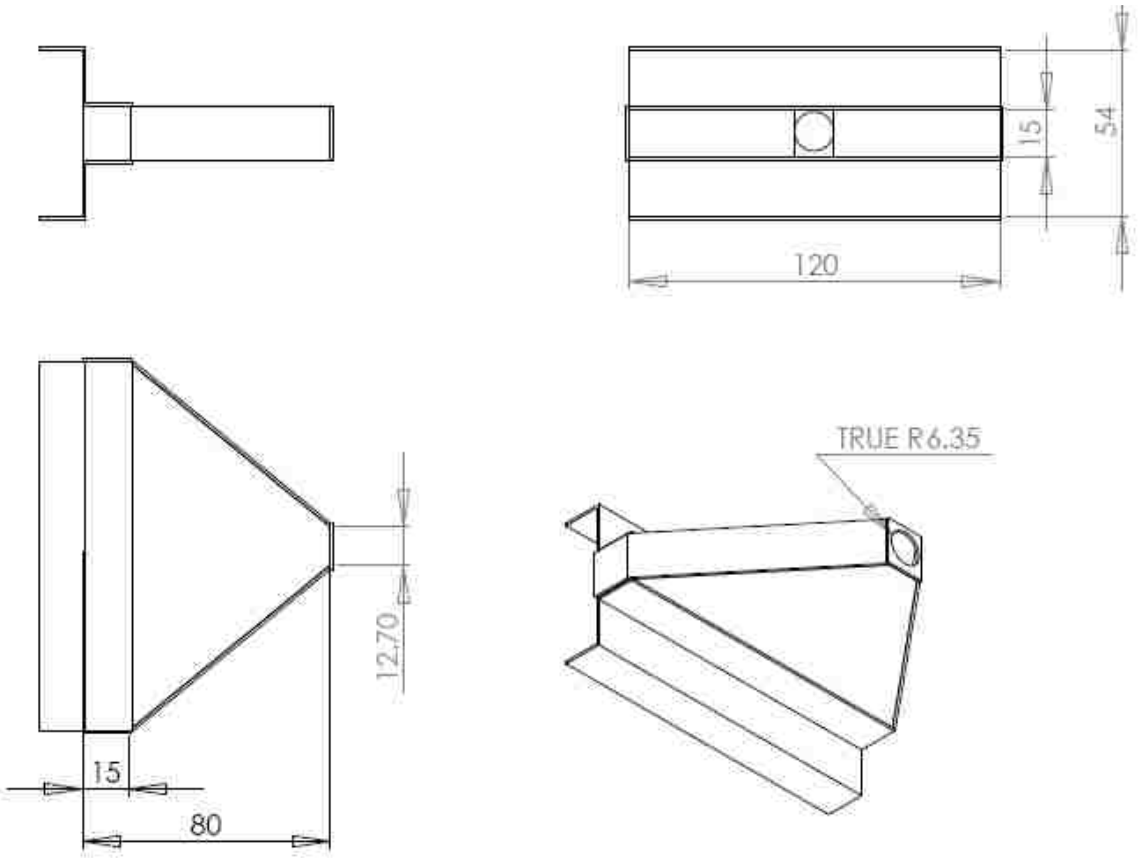

Figure 3.13. Nanocollector drawing detail with critical dimensions (in mm)

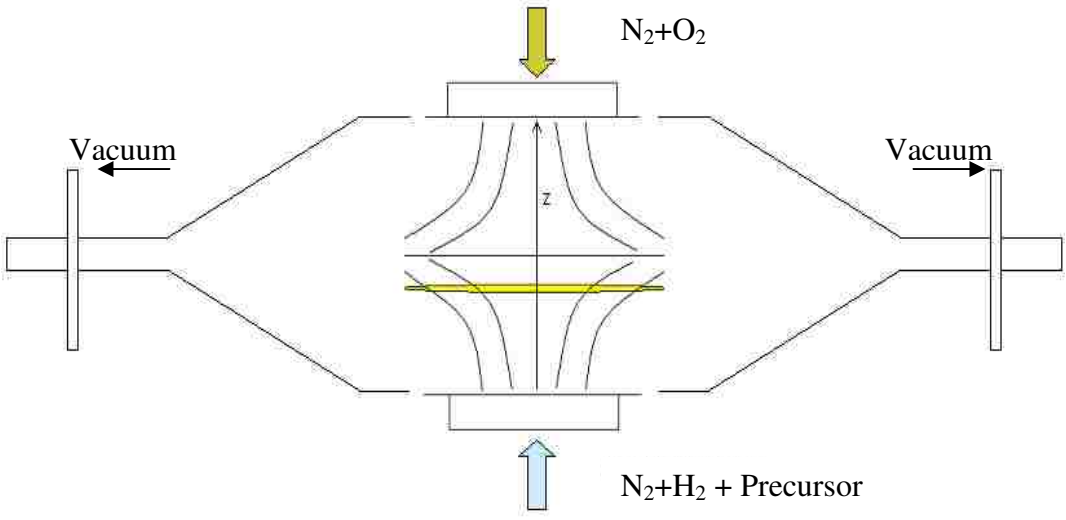

Figure 3.14. Schematic of the system nanocollector-CDF reactor.

In order to correlate the variation of synthesis conditions with the particle characteristics and efficiency of nanoparticles produced, a design of experiments (DOE-2) was performed. The DOE was designed based on Taguchi Design (L16, with 4 factors of 4 levels each one as indicated on table 3.7, 3.8 and 3.9). From preliminary experimentation the precursor-pumping rate was set constant at 250 [µl/h].

Each sample was obtained by collecting particles on a filter for every given condition set in the DOE-2 (see Table 3.7). Duplicated samples were obtained to account for reproducibility of the results. TEM grid samples were prepared by taking a dilute sample of particles from the filter and observed in the TEM of each experiment. The particle size distributions and the average particle size were calculated from the TEM images obtained. The Taguchi DOE the main effects plot of means for particle size are shown in Figure 3.15. A contour plot is shown in Figure 3.16 for the two main controlling factors on the particle size distribution, namely hydrogen flow rate and vacuum level. TEM images for the most representative samples from the DOE-2 are shown in Figures 3.16 and 3.21. Finally the particle size histograms for the same samples are presented in Figure s 3.17 to 3.20 and 3.22 to 3.24.

Table 3.7 Description of factors and levels used for DOE-2

Factor	Description / levels
H_2	flow rate of H_2 [L/min] levels: 2.00, 3.00, 4.00, 5.00
Vacuum	Vacuum [cm Hg] Levels: 8, 10, 12, 14
N_2/H_2	flow rate of N_2 in H_2 side [L/min] levels: 0.25, 0.50, 0.75, 1.00
N_2/O_2	flow rate of N_2 in O_2 side [L/min] levels: 0.25, 0.50, 0.75, 1.00

Note: O_2 flow rate set constant to 1 l/min (main channel)
and side channels as in table 3.8

Table 3.8 Description of factors and levels used for DOE-2

Side channels flow rate (L/min)			
O_2	N_2/O_2	N_2/H_2	H_2
0.85	3.61	0.00	2.72

Table 3.9 Gas Flow Conditions for DOE-2

Run	Vacuum [cm Hg]	Hydrogen [l/min]	N_2/H_2 [l/min]	N_2/O_2 [l/min]	mv ratio	Equivalent ratio	Average Size [nm]
1	8	2	0.25	0.25	0.0889	1.2770	53.48
2	10	2	0.5	0.5	0.0894	1.2770	55.24
3	12	2	0.75	0.75	0.0948	1.2770	45.23
4	14	2	1	1	0.1037	1.2770	47.37
5	8	3	0.5	0.75	0.1140	1.5475	48.87
6	10	3	0.25	1	0.0964	1.5475	47.38
7	12	3	1	0.25	0.1788	1.5475	35.41
8	14	3	0.75	0.5	0.1406	1.5475	36.99
9	8	4	0.75	1	0.1519	1.8179	32.39
10	10	4	1	0.75	0.1859	1.8179	25.54
11	12	4	0.25	0.5	0.1597	1.8179	37.52
12	14	4	0.5	0.25	0.1867	1.8179	31.20
13	8	5	1	0.5	0.2550	2.0884	27.56
14	10	5	0.75	0.25	0.2587	2.0884	19.86
15	12	5	0.5	1	0.1809	2.0884	23.45
16	14	5	0.25	0.75	0.1905	2.0884	28.00

Table 3.10. Values of volumetric flow rate in the reactor (Q_{cdf}), volumetric flow rate from infiltration (Q_{infil}), volumetric flow rate in the vacuum pump (Q_{Vacuum})

Run	Vacuum [in Hg]	Q_{Vacuum} [l/min]	Q_{cdf} [l/min]	Q_{infil} [l/min]
1	8	20.87	10.68	-10.19
2	10	18.38	11.18	-7.20
3	12	15.90	11.68	-4.22
4	14	13.42	12.18	-1.24
5	8	20.87	12.43	-8.44
6	10	18.38	12.43	-5.95
7	12	15.90	12.43	-3.47
8	14	13.42	12.43	-0.99
9	8	20.87	13.93	-6.94
10	10	18.38	13.93	-4.45
11	12	15.90	12.93	-2.97
12	14	13.42	12.93	-0.49
13	8	20.87	14.68	-6.19
14	10	18.38	14.18	-4.20
15	12	15.90	14.68	-1.22
16	14	13.42	14.18	0.76

3.6.1. Effect of Flame Synthesis Conditions on particle size. From Figures 3.15 and 3.16 it can be inferred that the main effect on particle size was due to variations on hydrogen flow rate. Hydrogen flow rate mainly controls the flame's temperature; therefore as hydrogen flow rate increases, flame temperature increases (providing there is an excess of oxygen as in the present setup). The higher the flame temperature, the more energy that is available to decompose the precursor and form the initial agglomerates at the bottom of the stagnation layer. It is necessary to take into account that increasing the hydrogen flow rate also increases the gas velocity and therefore particles formed inside the stagnation layer travel faster toward the flame. The combined effect of faster velocity and higher temperature yield the production of smaller particles. The results of increasing nitrogen flow rate in the hydrogen's side (N_2/H_2 parameter in Figure 3.15) show that the overall trend is to reduce particle size as gas momentum ratio increases. This result corroborates the hypothesis that higher gas velocity in the precursor's gas stream (hydrogen's side) can decrease particle size. On the other hand, the opposite effect is observed when nitrogen flow rate in the oxygen side is increased (Figure 3.15 a).

Vacuum conditions also have an effect in reducing particle size, but in a minor scale compared to hydrogen flow rate variations. The gas volumetric balance ($Q_{balance}$) in the nanocollector is shifted when vacuum is present (Figure 3.15, 3.16). As described before, the vacuum level is inversely proportional to the gas flow rate passing through the pump. As vacuum increases, gas flow rate decreases. The main effect plot indicates that as vacuum increases, the average particle size decreases and reaches a minimum at vacuum equal to 12 inch of Hg. The average particle size slightly increases after reaching the minimum, indicating a $Q_{balance}$ shifting from low vacuum to low-pressure differential as estimated in Table 3.10.

With respect to the N_2 flow rate in the hydrogen side, N_2/H_2 (see Figure 3.15), as this gas flow rate increases, the average particle size proportionally decreases to a minimum of around 35 nm at 0.75 l/min. In the oxygen side, when N_2/O_2 increases the particle size increases up to or max value of about 40 nm at 0.50 l/min.

Increments of N_2 flow rate in the hydrogen side increase the momentum and the flame combustion is accelerated providing there is excess of oxygen with particle size

decreasing accordingly. N_2 flow rate increments in a flame with excess of hydrogen do not result in further flame temperature increments and particle size is unaffected.

For N_2 in the oxygen side the results are similar to the above case, but in this case a maximum is observed. The increments of N_2 flow rate results in a lower position of the stagnation layer as well as smaller velocities in the Z component, that is particles experience larger residence time that eventually results in a larger particle size.

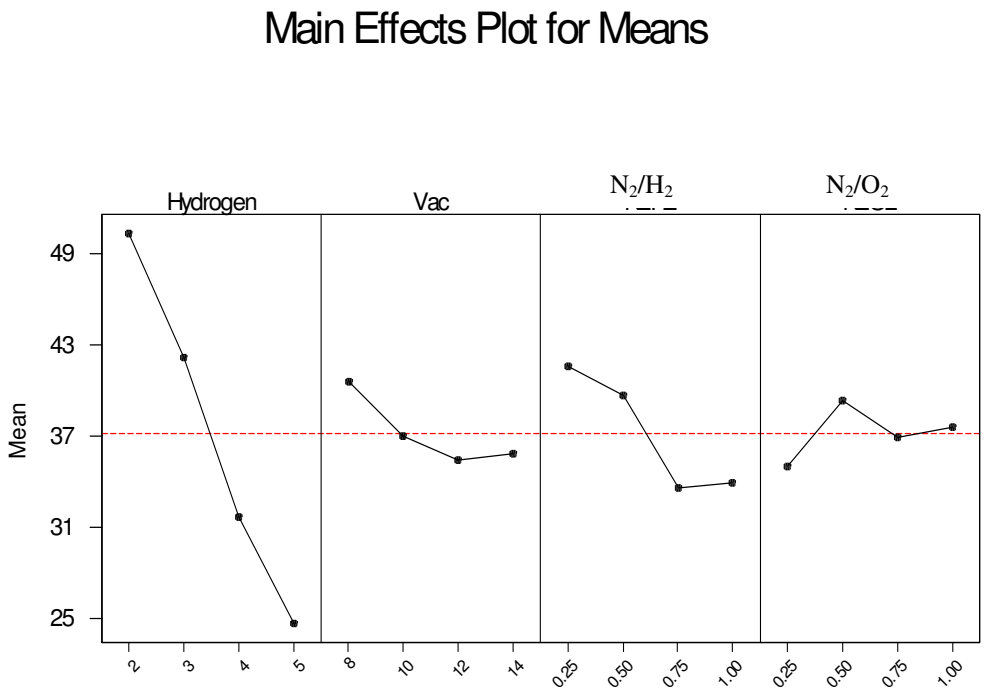

Figure 3.15. Main effect plot of means for particle size using the nanocollector - flame reactor system.

Figure 3.15 presents the main effect data obtained from the DOE-2 for average particle size as a function of the two parameters that are more significant to control particle size, namely, vacuum and hydrogen flow rates. The contour can be divided in four quadrants. In the first quadrant, low levels of both vacuum and hydrogen flow rate are present. The average particle size reaches a maximum value of around 50 nm. The flame conditions are at lower equivalence and momentum ratios. Flame reducing

conditions are increasing as hydrogen flow rate increases. Thus particles produced under these conditions would observe a maximum growth for the experimental range tested.

In the second quadrant, high hydrogen flow rate and low vacuum levels are present. The average particle size is around 40 nm. The effect of vacuum is observed when compared with the previous quadrant. The total momentum that particles experience is at a middle level, low enough that some particle-growth is achieved.

For the third and fourth quadrants, high hydrogen flow rates dominate the average particle size obtained. The high level of momentum in the hydrogen stream allows faster residence time, thus the particle size is reduced compared with all other conditions; the minimum particle size of 30 nm is achieved for the range of flame-vacuum conditions tested.

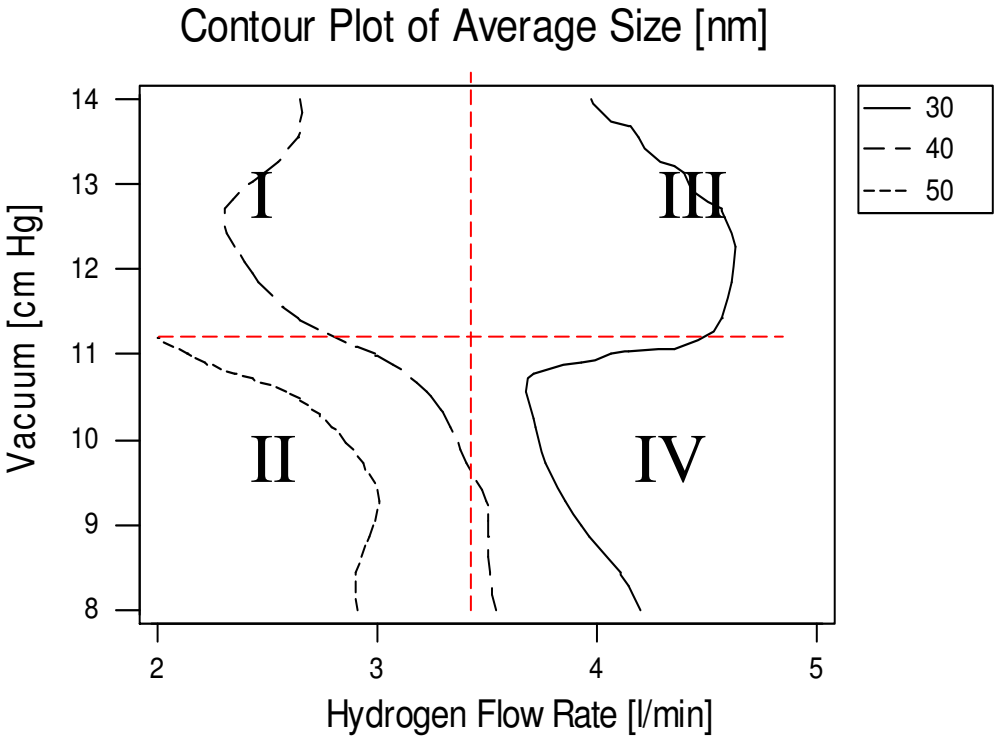

Figure 3.16. Contour plot for particle size as function of different levels of vacuum and hydrogen flow rate.

Figure 3.17 shows the TEM images for runs # 1, 2, 7 and 13. Runs 1 and 2 (Figure 3.17 a, b) represent flame conditions where lower hydrogen flow rate and low vacuum are present. That is they represent conditions from the first quadrant in Figure 3.16, where the average particle size is at its maximum of around 50 nm. Figure 3.17a may differ slightly from Figure 3.17b (run #2). Both samples show the presence of agglomerates besides single nanoparticles. The level of vacuum is inversely proportional to the flow rate passing through the pump (see appendix A). Therefore at this condition both agglomerates and single nanoparticles are transported to the filter.

Comparing the samples from runs 1 and 2 with samples in runs # 7 and 13 (images c) and d) with Figure 3.17, the average particle size is smaller, mainly due to lower hydrogen flow rates in runs 7 and 13. In particular, the sample from run 13 does not possess agglomerates but only single nanoparticles. The vacuum condition for this sample was at the same level as run 1, thus the difference in presence of agglomerates should come from the flame conditions. Both nitrogen gas flow rates are higher in run 13 compared to run 1 (see table 3.8). The higher the gas flow rate in this run, the more likely it is associated with a more complete evolution of the agglomerates into nanoparticles in run 13 compared with others samples in Figure 3.17. It can be quantified by the momentum ratio of 0.2550, around 3 times bigger than the values for runs 1 and 2.

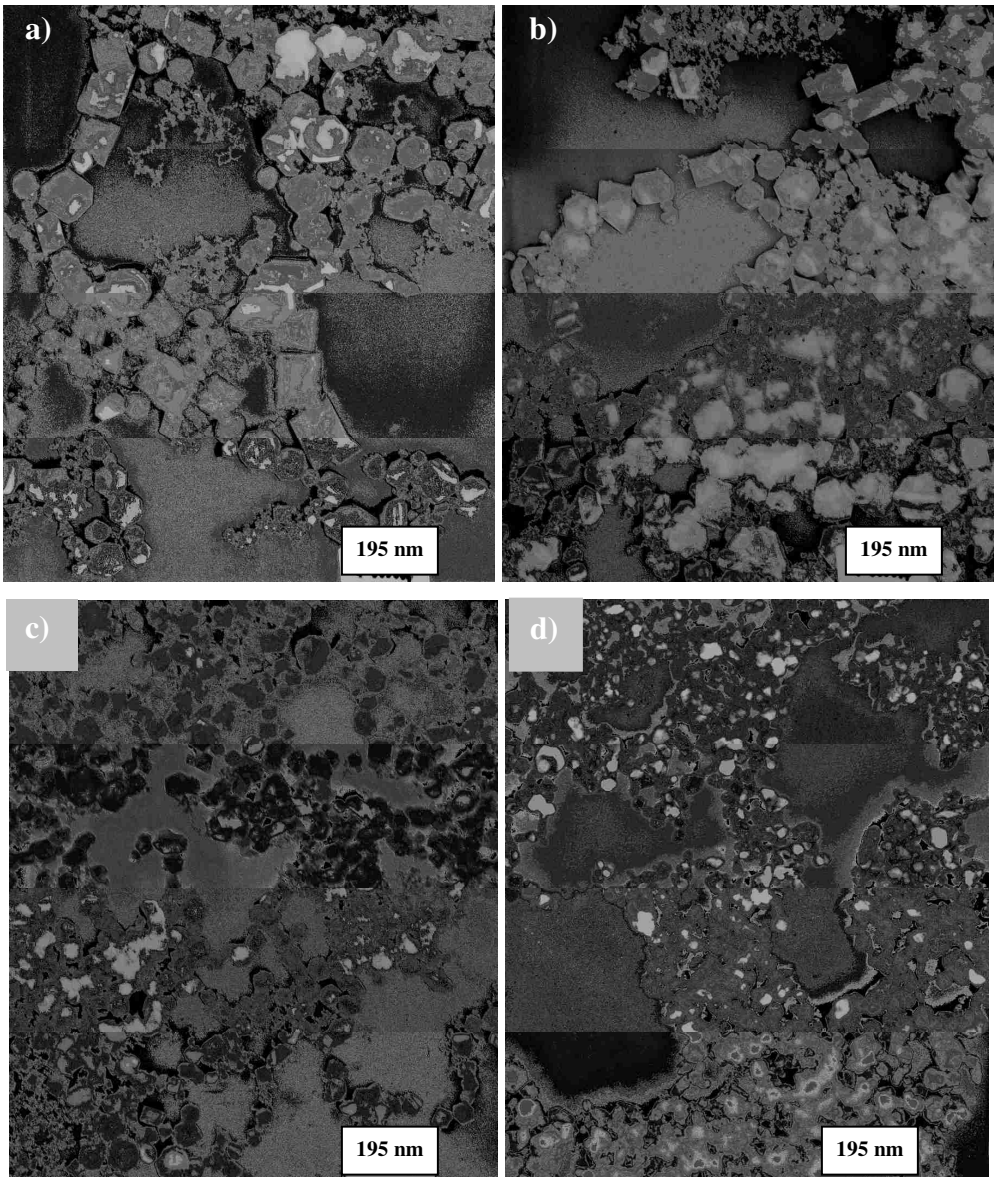

Figure 3.17. TEM images for run # 1, 2,7,13 (images a, b, c and d). Notice average particle size decreases from 51.4-55.2 nm (a, b) to 33.6 nm (c) and finally 28.14 nm (d). Agglomerates are present mostly in all images but d. Cubic particles are also present in images (a).

Figures 3.18 to 3.21 show the particle size distribution histogram and normal curve for samples in Figure 3.17. Runs # 1 and 2 show an average particle size of 51.4 and 55.2 nm, respectively, with the sample in run #1 presenting a secondary peak of large particles at 90 nm (see Figure 3.18). This could indicate a binary particle size distribution. Run # 2 also shows three secondary peaks at 40, 65 and 90 nm. On the other hand, samples for run 7 and 13 present an average particle size of 33.6 and 28.1 nm, respectively. The particle size distribution in run # 7 (Figure 3.20) shows a broader distribution of sizes, while run # 13 particle size distributions is shifted to values in the 20 nm range.

Comparing the results, the particle size distribution in samples with larger average particle size presents binary and ternary distributions (run 1 and 2, Figures 3.18 and 3.18). Samples with smaller average particle size (runs 7 and 13, Figure 3.20 and 3.21) have a particle size distribution more normalized, i.e. the distribution shows a histogram evenly distributed around an average particle size. That means the distribution does not present multi-modal size modes in runs with smaller average particle size (runs 7 and 13). Nonetheless the samples analyzed possess a narrow particle size distribution with a broader distribution around the average value. These characteristics in the particle size distribution suggest that the nanoparticle formation was observed in a range of flame conditions.

The characteristic in the particle size distribution points out the variability of the formation process. Thus the results are indicative that different particles form in different synthesis conditions. Particles could be exposed to a range of synthesis conditions in the flame, and as a result they do form and grow in a multiple set of environmental conditions inside the reactor.

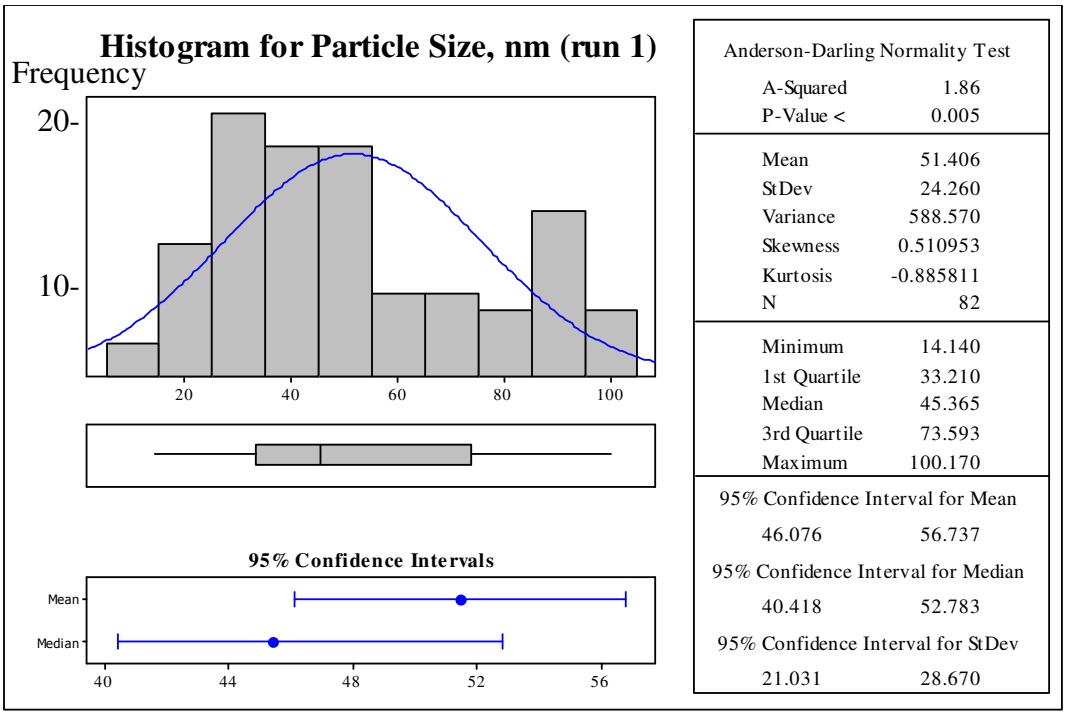

Figure 3.18. Histogram and descriptive statistic DOE-2 run 1.

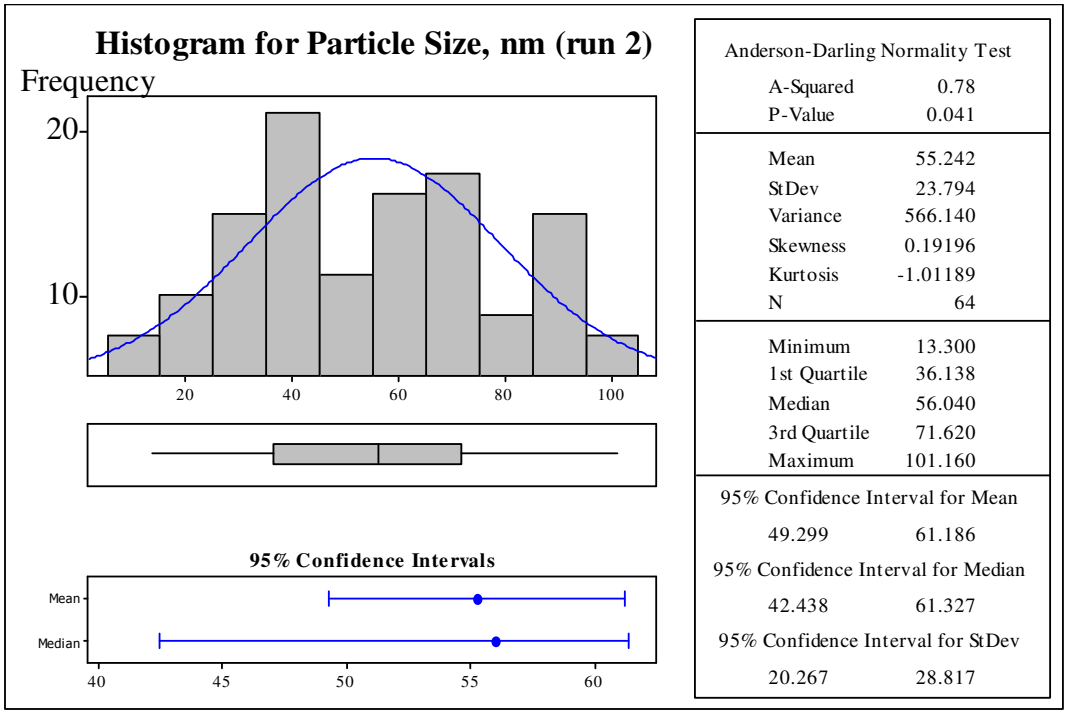

Figure 3.19. Histogram and descriptive statistic DOE-2 run 2.

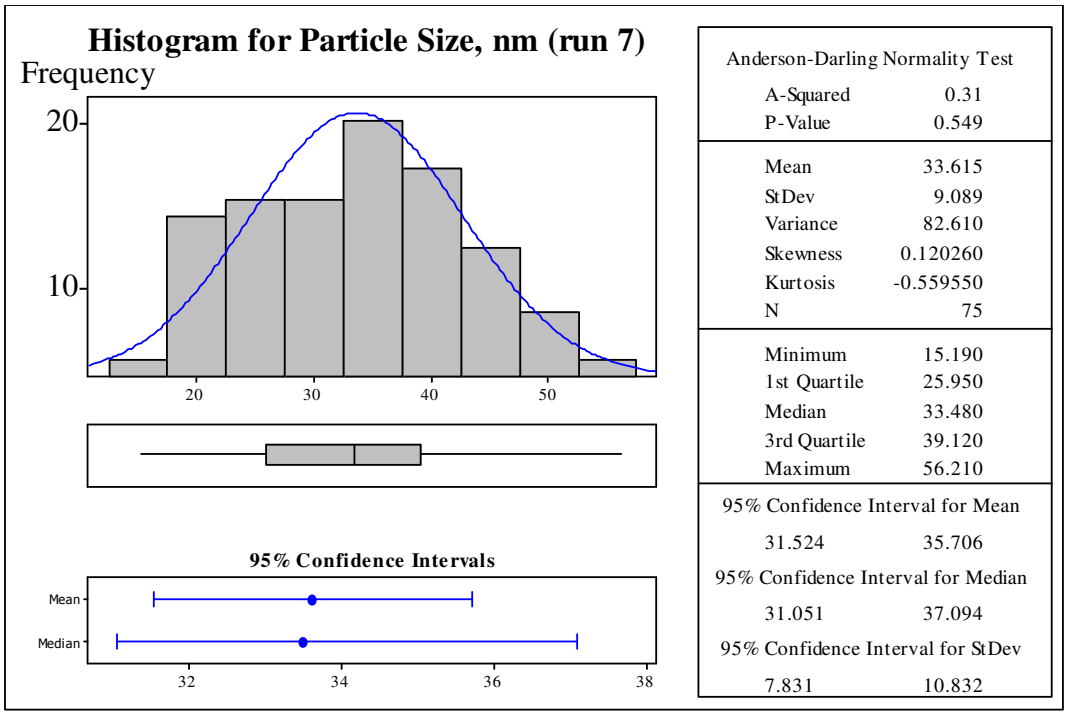

Figure 3.20. Histogram and descriptive statistic DOE-2 run 7.

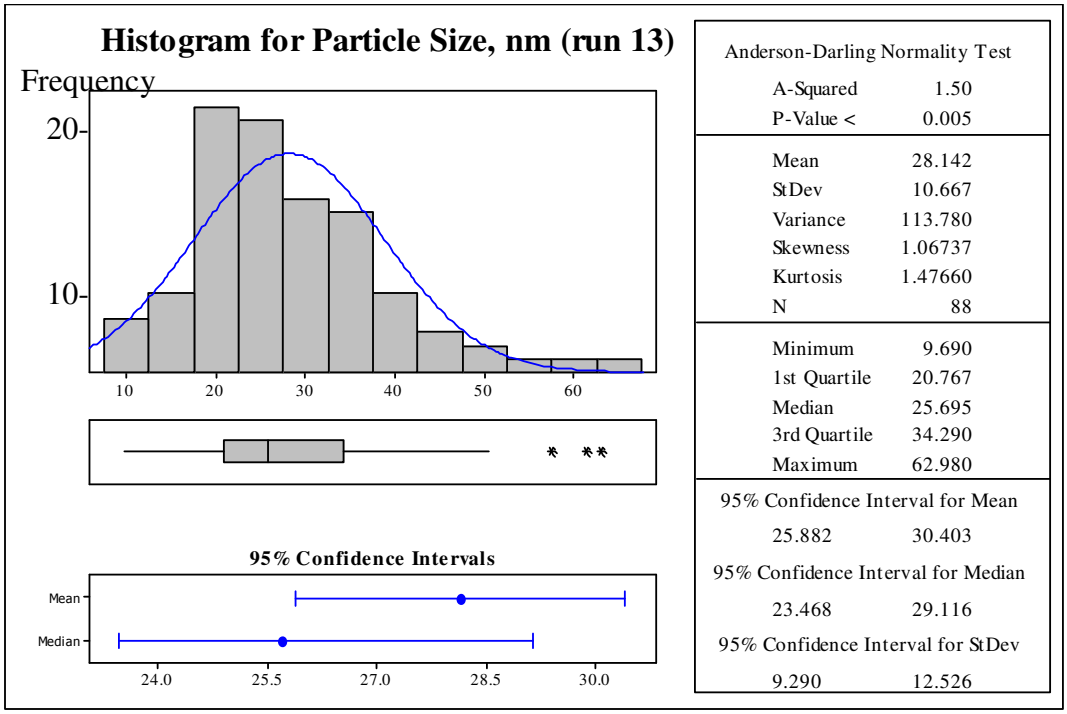

Figure 3.21. Histogram and descriptive statistic DOE-2 run 13.

Figure 3.22 shows the TEM results for runs # 4, 7 and 9. Again, in this figure it is observed a trend decreasing average particle size from 50 nm in run 4 (Figure 3.22a) up to 30 nm (Figure 3.22d). It can be observed the presence of mostly hexagonal nanoparticles in all samples.

As in runs 1 and 2 in Figure 3.17, run # 4 in Figure 3.22 is in the first quadrant (see Figure 3.15), where particle size average is at its maximum of around 50 nm. Conditions that control the particle size are mainly low hydrogen flow rate compared with conditions in runs 7 and 9.

Run # 9 (Figure 3.22 c) does not show the presence of agglomerates. Examining the gas flow rate conditions, the momentum ratio is 1.7 times higher than in runs 4 and 7. Thus the higher the gas flow rate in this run most likely is associated with a more complete evolution of the agglomerates into nanoparticles in run 9 compared with other runs in Figure 3.22.

In summary from the results in Figure 3.17 to 3.24, the particle size is mainly controlled by the hydrogen flow rate. The amount of agglomerates collected is mainly related to the combined effect of the gase flow rate. For higher flow rates in the flame the momentum ratio is larger and this parameter controls how fast the agglomerates are transported and destroyed to form single nanoparticles.

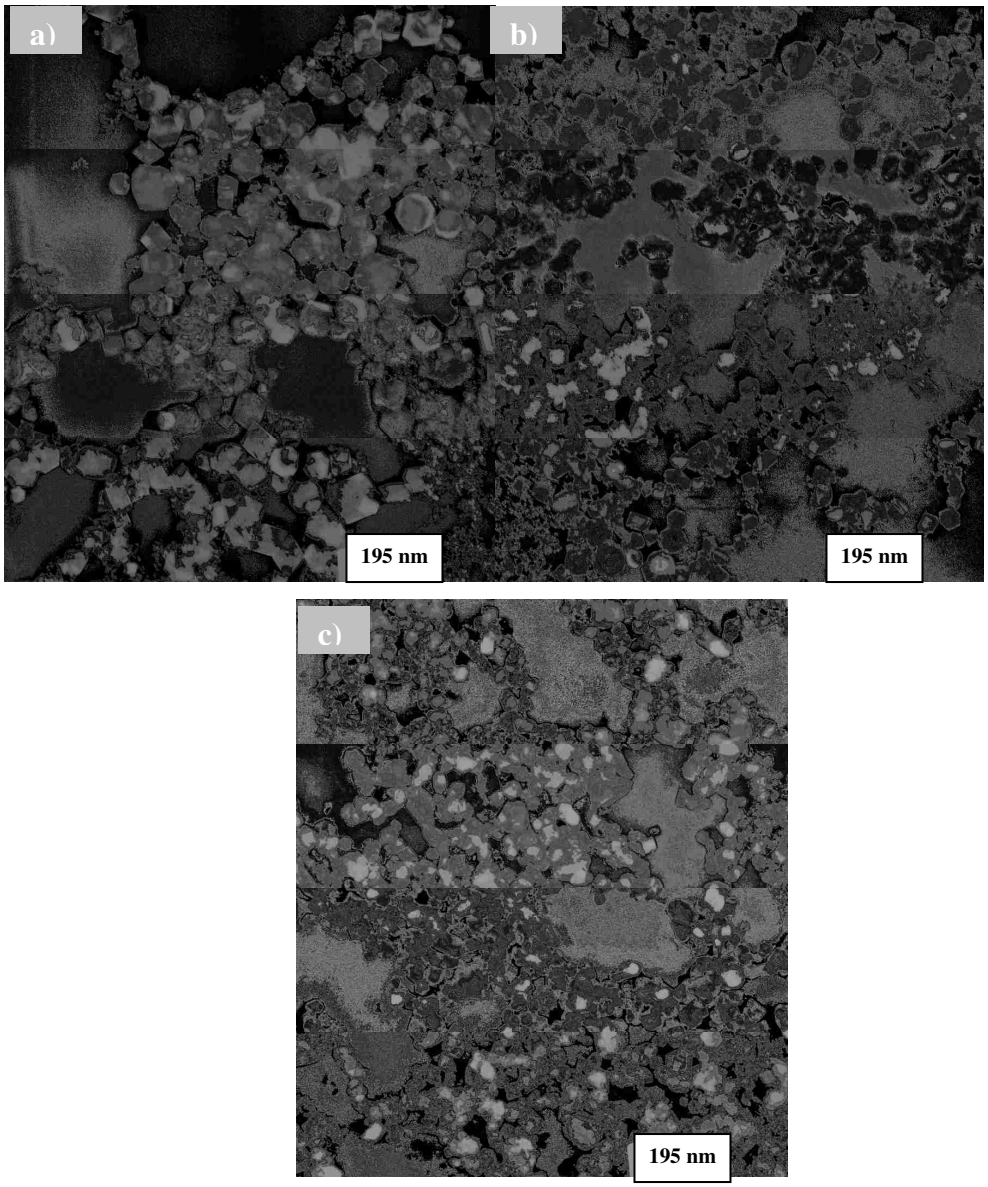

Figure 3.22 TEM images for run # 4,7,9 (images a, b and c). Notice average particle size decreases from 50 nm (a) to 40 nm (b) and finally 30 nm (c). Agglomerates are present mostly in all images but c.

Figures 3.23 and 3.24 present the particle size distribution and normal curve for samples in Figure 3.22. Run 4 (Figure 3.23) shows a particle size distribution with average particle size of 50.5 nm while run 9 (Figure 3.24) has an average particle size of 32.4 nm. The sample for run 4 shows a well developed and normalized distribution towards the average particle size as mentioned above. The median of the distribution is 48.9 nm in run 4, shifted toward a value slightly smaller than the average size for this distribution.

In run # 9 (Figure 3.24) the average particle size is 32.36 nm. The median is shifted to a value of 30.64 nm. This means the distribution is skewed towards a smaller particle size as in run 4 (Figure 3.23), suggesting also the presence of a broader band of synthesis conditions.

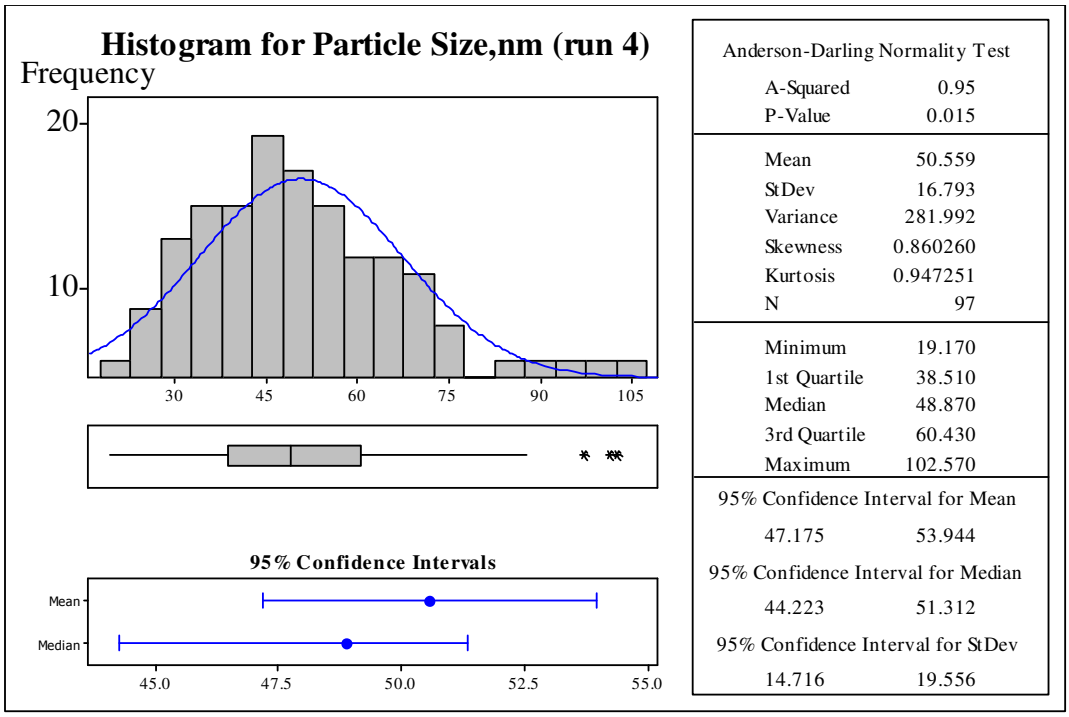

Figure 3.23. Histogram and descriptive statistic DOE-2 run 4.

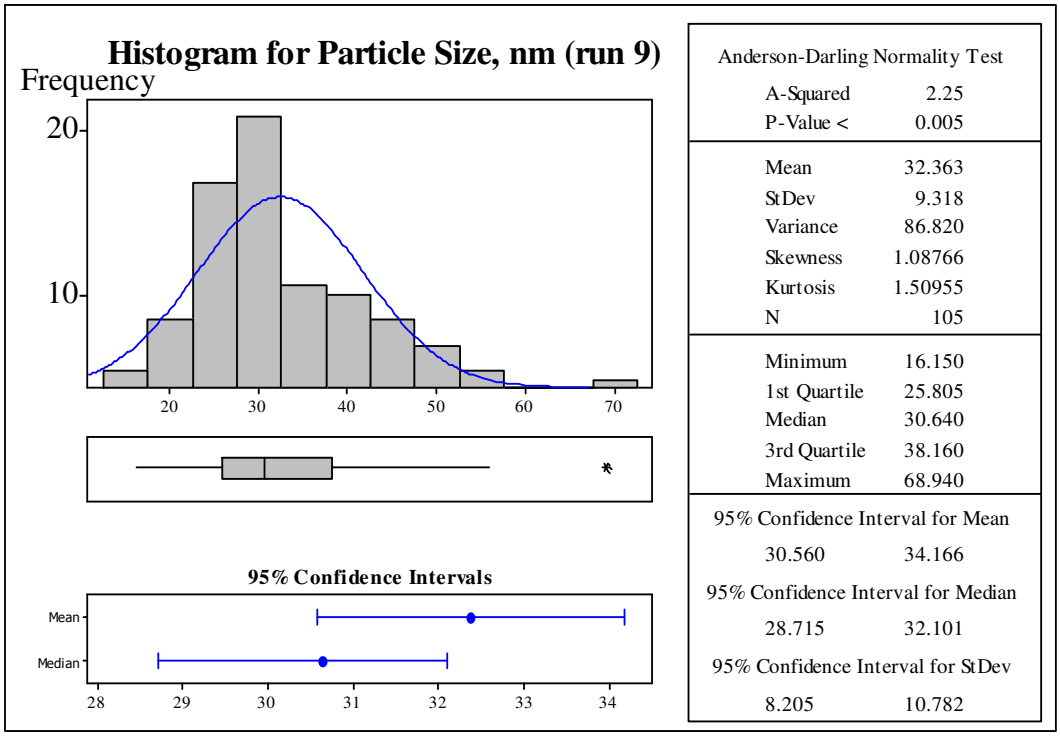

Figure 3.24. Histogram and descriptive statistic DOE-2 run 9.

4. CONCLUSIONS

From the experimental results, it was inferred of the main factors that control the synthesis conditions of iron oxide nanoparticles in CDF reactor. The results show the importance of the factors as follows.

Hydrogen flow rate have the highest importance among all other control factors studied with respect to flame structure, temperature control, and final nanoparticles characteristics. The effect of hydrogen flow rate was the direct control of the flame temperature profiles, gas flow momentum ratio and atmosphere conditions related by the equivalence ratio. The combined control effect of hydrogen flow rate in the parameters mentioned above was the key ingredient in developing the final nanoparticle characteristics studied, namely, the shape and particle size.

In section 3.3 and 3.4 the flame structure was studied for its changes as a function of the precursor rate as well as the hydrogen flow rate. It was found that increments in precursor rate affect the structure of the flame. The flame lower limit height increases and at the same time, the stagnation layer becomes larger and wider. The flame upper limit remains almost unchanged and the changes in the flame structure are mainly associated with a partial cooling of the flame as precursor rate increases.

On the other hand, increments in the hydrogen flow rate at constant precursor flow rate can be particularly useful to control both flame structure and temperature profile. It was shown that at relatively low values of hydrogen flow rates the upper limit of the stagnation layer can overlay the flame and under such conditions nanoparticles experience both high temperatures and comparatively larger residence times. The result of applying such synthesis conditions is the selective formation of mostly hexagonal nanoparticles with a narrow size distribution and an average size around 20 nm.

With respect to the control factors of nanoparticle shape formation, the formation of cubic nanoparticles was characterized. It was found that the mechanism of formation of cubic nanoparticles is associated with the equivalence ratio and in a lesser extent by the momentum ratio. Since both parameters are directly controlled by the hydrogen flow rate (with all others parameters constant), the variations in hydrogen flow rate greatly affect the formation of cubic nanoparticles. It was observed a minimum of cubic particles

around 2.95 to 3.66 l/min of hydrogen flow rates (equivalence ratio of 0.749 and 0.928 respectively) and low momentum ratio values (0.4565 to 0.4920).

The main parameters for controlling the formation of cubic-shape nanoparticles were found to be the equivalence ratio and temperature profile. With excess of oxygen the higher the hydrogen flow rate is, the higher the temperature obtained and the smaller the number of cubic nanoparticles formed. As flame conditions approach to stoichiometry, a minimum amount of cubic nanoparticle were found, due mainly to maximum temperatures in the flame. At conditions when lower flame temperatures were generated, the percentage of cubic nanoparticles increases.

The percentages of cubic nanoparticles are relatively low compared to the ones found for hexagonal nanoparticles. The main reason for this behavior was associated to the fact that in diffusion flames, the flame is formed by diffusion of fuel on one side and oxidant in the opposite side. At some point in the flame there is always a stoichiometric mixture. Strong reducing/oxidizing conditions inside the flame are not possible and therefore the selective formation of 100 % cubic nanoparticles may not be possible in the CDF reactor. On the other hand, stoichiometric conditions favor formation of hexagonal nanoparticles. The fact that there is always a local stoichiometric condition in the flame favors the formation of hexagonal particles.

With respect to the particle size distribution and average particle size, results shows a clear trend in reducing the average particle size as the hydrogen flow rate increases. The main effect on particle size was observed due also to hydrogen flow rate. A secondary minor effect was observed for variation of other parameters as vacuum flow rate, N_2 flow rate in the H_2 stream and last N_2 Flow rate in the O_2 side. The effect of vacuum level on particle size can be associated to changes in the total mass/volumetric flow rate balance.

On the other hand, using the nanocollector the particle size distributions for samples in section 3.6 are wide spread and in some cases they show a bimodal or tri-modal particle size distribution. This characteristic was mainly associated with the variability in the synthesis conditions in this particular setup.

Themophoresis was found to be important for increasing nanoparticle collection efficiency. A maximum percentage of nanoparticles of all shapes collected was found by preheating the probe temperature to 200 °C.

APPENDIX

PRESSURE – VACUUM CURVE FOR OIL LESS DIAPHRAGM UNIT USED IN SECTION 3.6

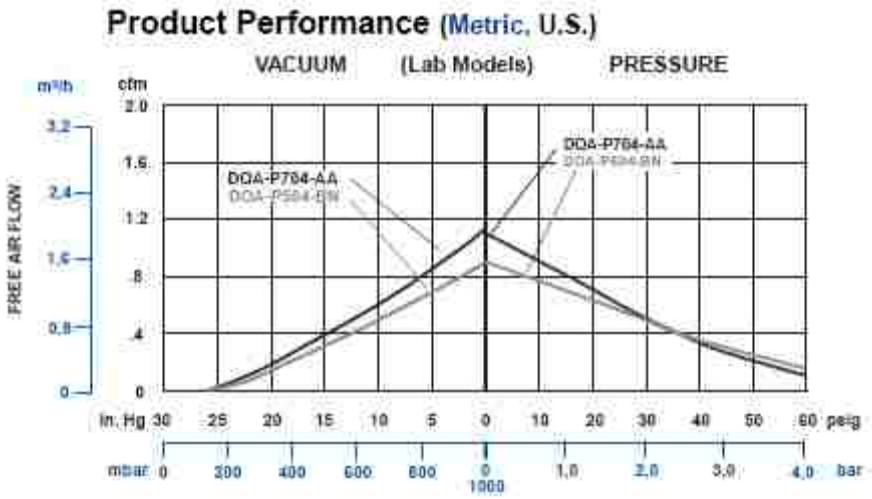

Figure A1. Pressure – Vacuum curve for Oil less Diaphragm pump 1.9-cfm/3,23 m^3

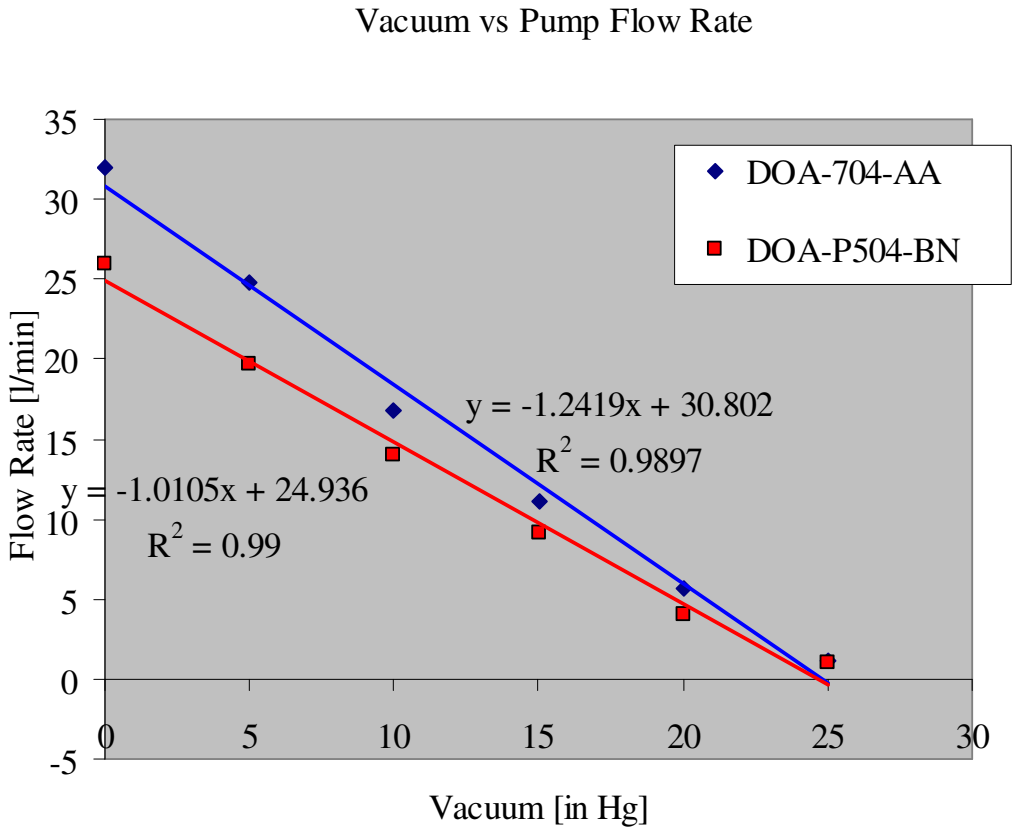

Figure A2. Pressure – Vacuum curve for Oil less Diaphragm pump1.9 cfm/3,23 m^3/h

BIBLIOGRAPHY

[1] http://itri.loyola.edu/nano/IWGN.Research.Directions/. "Nanotechnology Research Directions," M.C. Roco (editor). IWGN workshop, July 2008.

[2] Alke Petri-Fink & and Heinrich Hofmann, "Superparamagnetic iron oxide nanoparticles (SPIONs): From synthesis to in vivo studies - A summary of the synthesis, characterization, in vitro, and in vivo investigations of SPIONs with particular focus on surface and colloidal properties". IEEE Transactions on Nanobioscience, 6 (2007), 289-297.

[3] Jing, Zhihong. "Preparation and magnetic properties of fibrous gamma iron oxide nanoparticles via a nonaqueous medium". Materials Letters. 60 (2006). 2217-2221.

[4] T. Gonzalez-Carreno, M.P. Morales, M. Garcia and C.J. Serna. "Preparation of uniform gamma- Fe_2O_3 particles with nanometer size by spray pyrolysis". Materials Letters 18 (1993) 151-155.

[5] B. Martinez et al. "Magnetic characterization of gamma- Fe2O3 nanoparticles fabricated by aerosol pyrolysis". Journal of Applied Physics. 83 (1998), 3256-3262.

[6] S. Veintemillas-Verdaguer, M.P. Morales, C.J. Serna. "Continuous production of gamma- Fe_2O_3 ultrafine powders by laser pyrolysis". Materials Letters 35 (1998) 227-231.

[7] http://www.azonano.com/Details.asp?ArticleID=1600#_Gas-Phase_Synthe. "Nanostructured Materials Production and Manufacturing in Order To Gain Special Effects and Properties". July 2008.

[8] M.R. Zachariah, M.I. Aquino, R.D. Shull and E.B. Steel. "Formation of superparamagnetic nanocomposites from vapor phase condensation in a flame". NanoStructured Materials, 5 (1995) 383-392.

[9] Y.Xing, T.P. Kole and J.L. Katz. "Shape-controlled synthesis of iron oxide nanoparticles". Journal of Materials Science Letters, 22 (2003) 787-790.

[10] Dixon-Lewis and G.L. Isles. " Flame structure and flame reaction kinetics III. Measurement of temperature profiles in flames at atmospheric pressure" Proc. Roy. Soc. A. 308 (1969) 517-536.

[11] M. D. Rumminger and G. T. Linteris. "The Role of Particles in Counterflow Diffusion Flames Inhibited by Iron Pentacarbonyl," Combustion Institute Joint Meeting. Proceedings. March 26-28, 2001, Oakland, CA.

[12] B. Guo and Ian M. Kennedy. “Gas-Phase Flame Synthesis and Characterization of Iron Oxide Nanoparticles for Use in Health Effects Study,” Aerosol Science and Technology. 41 (2007) 944-951.

[13] A.W. D. Hills and A. Paulin. “The construction and calibration of an inexpensive microsuction pyrometer”. Journal of Scientific Instruments (Journal of Physics E), 2 (1969) 713-717.

[14] Y. Yang, L. Li, G. Chen, E. Liu. “Synthesis and characterization of iron-based alloy nanoparticles for magnetorheological fluids”, Journal of Magnetism & Magnetic Materials, 320 (2008) 2030-2038.

[15] O. Acarbas, M. Ozenbas. “Preparation of iron oxide nanoparticles by microwave synthesis and their characterization” Journal of Nanoscience & Nanotechnology, 8 (2008) 655-659.

[16] U. T. Lam, R. Mammucari, K. Suzuki, N.R. Foster, “Processing of iron oxide nanoparticles by supercritical fluids” Industrial & Engineering Chemistry Research. 47 (2008) 599-614.

[17] C.M. Sorensen, W. B. Hageman, T.J. Rush, H. Huang, and C.Oh. “Aerogelation in a flame soot aerosol”. Physical Review Letters. 80 (1998) 1782-85.

VITA

Hector Enrique Ruiz was born on December 29, 1962, in Caracas, Venezuela. He received his primary and secondary education in Caracas, Venezuela and his Bachelor of Science Degree in Materials Engineering from The Department of Materials Science, University Simon Bolivar, in December 1994.

Hector served as a Research Assistant at the Research Institute FUNINDES, University Simon Bolivar; Research Student at the Ecole Nationale Supérieure de Ceramique Industriel (ENSCI), Limoges, France. He was Graduate Research Assistant at University of Missouri-Rolla.

He worked as Technical Researcher at INTEVEP S.A., Materials Technology Department, Los Teques - Venezuela, Assistant manager at the Ceramica Carabobo Corporation, Refractories Division, Valencia - Venezuela and as Instructor at the Technology Institute IUT-RC, Caracas –Venezuela. He also worked as Research Engineer at MO-Sci Corporation, in Rolla, Missouri and as Consultant in Product Development at DOTEC Engineering, in St Charles, Missouri.

Hector has been a student member of the American Ceramic Society, American Society of Materials (ASM), the Minerals Metals & Materials Society, the Iron & Steel Society, and the Mineralogical Society of America, the American Society of Chemical Engineers.